Mineralium Deposita (2020) 55:515–534
https://doi.org/10.1007/s00126-019-00890-8

ARTICLE

Magma generation and sulfide saturation of Permian mafic-ultramafic intrusions from the western part of the Northern Tianshan in NW China: implications for Ni-Cu mineralization

Yu-Feng Deng[1,2,3] · Feng Yuan[1,2,4] · Peter Hollings[1,5] · Xie-Yan Song[6] · Taofa Zhou[1,2] · Bin Fu[7] · Steven Denyszyn[3] · Bingbing Zhao[1]

Received: 21 March 2018 / Accepted: 21 April 2019 / Published online: 28 May 2019

Abstract

Compared to Permian magmatic Ni-Cu sulfide deposits in the eastern part of the Northern Tianshan, such as Huangshan and Huangshandong, those in the western part (e.g., Baixintan and Lubei) are poorly documented. Zircon ID-TIMS U-Pb age data (279.7 ± 0.2 Ma) of lherzolite and LA-ICPMS U-Pb age data (277.8 ± 3.4 Ma) of a hornblende gabbro suggest the Lubei intrusion was emplaced in the Early Permian. The Baixintan and Lubei mafic-ultramafic intrusive rocks are characterized by enrichments of large ion lithophile elements and Th and U relative to the high field strength elements, as well as depletion of Nb and Ta relative to mid-ocean ridge basalt. The $(^{87}Sr/^{86}Sr)_t$ (0.70354–0.70713), $\varepsilon Nd_{(t)}$ (2.80 to + 7.05), and $\varepsilon Hf_{(t)}$ (2.50–18.4) values for the intrusions indicate that they have assimilated Tianshan basement rocks, whereas the Se/S ratios (181×10^{-6}–418×10^{-6}) and $\delta^{34}S_{CDT}$ values (− 0.13‰ to 0.90‰) of the sulfides suggest that crustal sulfur has not been incorporated into the magma. The decrease in Pd/Zr with increasing $(Th/Nb)_{PM}$ indicates that sulfide saturation accompanied crustal contamination. The olivine compositions and whole-rock chalcophile elements of the Baixintan and Lubei intrusions imply that the parental magma of the intrusive rocks in the west contains higher chalcophile elements than those in the east, which suggests that the mafic-ultramafic intrusions in the western part of the Northern Tianshan should be regarded as favorable Ni-Cu sulfide exploration targets.

Keywords Magmatic Ni-Cu sulfide deposit · Baixintan mafic-ultramafic intrusion · Lubei mafic-ultramafic intrusion · Western Northern Tianshan · Mantle source · Sulfide saturation

Editorial handling: M. Fiorentini

Electronic supplementary material The online version of this article (https://doi.org/10.1007/s00126-019-00890-8) contains supplementary material, which is available to authorized users.

✉ Yu-Feng Deng
dyfeng_214@sina.com

[1] Ore Deposits and Exploration Centre, School of Resources and Environmental Engineering, Hefei University of Technology, 193th Tunxi Road, Hefei 230009, Anhui Province, China

[2] Anhui Province Engineering Research Center for Mineral Resources and Mine Environments, Hefei 230009, China

[3] Centre for Exploration Targeting (CET), ARC Centre of Excellence for Core to Crust Fluid Systems, The University of Western Australia, Crawley, WA 6009, Australia

[4] Xinjiang Research Centre for Mineral Resources, Xinjiang Institute of Ecology and Geography, Chinese Academy of Sciences, Urumqi 830011, Xinjiang, China

[5] Department of Geology, Lakehead University, 955 Oliver Road, Thunder Bay, ON P7B 5E1, Canada

[6] State Key Laboratory of Ore Deposit Geochemistry, Institute of Geochemistry, Chinese Academy of Sciences, Guiyang 550002, China

[7] Research School of Earth Sciences, The Australian National University, Canberra 0200, Australia

Introduction

In the past decades, a growing number of magmatic Ni-Cu sulfide deposits have been found in plate margin settings, such as Xiarihamu (China), Santa Rita (Brazil), Aguablanca (Spain), Quetico (Canada), and Duck Island (USA), indicating significant exploration potential in this tectonic environment (Tornos et al. 2001; Pettigrew and Hattori 2006; Thakurta et al. 2008; Maier et al. 2008; Ripley 2009; Barnes et al. 2011; Xie et al. 2014; Li et al. 2015; Song et al. 2016). Magmatic Ni-Cu sulfide deposits hosted by Permian mafic-ultramafic intrusions in the Northern Tianshan along the southern margin of the Central Asian Orogenic Belt (CAOB) contain roughly 1 million metric tons (Mt) of Ni metal reserves (Fig. 1; Qin et al. 2003; Liu et al. 2005; Su et al. 2013). Magmatic Ni-Cu sulfide deposits in the eastern part of the Northern Tianshan include Huangshan, Huangshandong, Tulaergen, Huangshannan, Xiangshan, Tudun, and Hulu (Zhang et al. 2011; Sun et al. 2013; Tang et al. 2014; Deng et al. 2014, 2017; Wang et al. 2015; Mao et al. 2015, 2017a). Most of the intrusions that host magmatic Ni-Cu sulfide deposits in the eastern part of the Northern Tianshan formed around 280 Ma (Zhou et al. 2004; Mao et al. 2008; San et al. 2010; Qin et al. 2011; Song et al. 2013; Zhao et al. 2016), due to the interaction between metasomatized lithospheric mantle and ascending asthenospheric mantle, as a result of slab break-off or an upwelling mantle plume (Zhou et al. 2004; Qin et al. 2011; Su et al. 2011; Gao and Zhou 2012; Gao et al. 2013; Song et al. 2013; Deng et al. 2015). Although crustal contamination is generally accepted to have been critical in triggering sulfide segregation to form the deposits, fractional

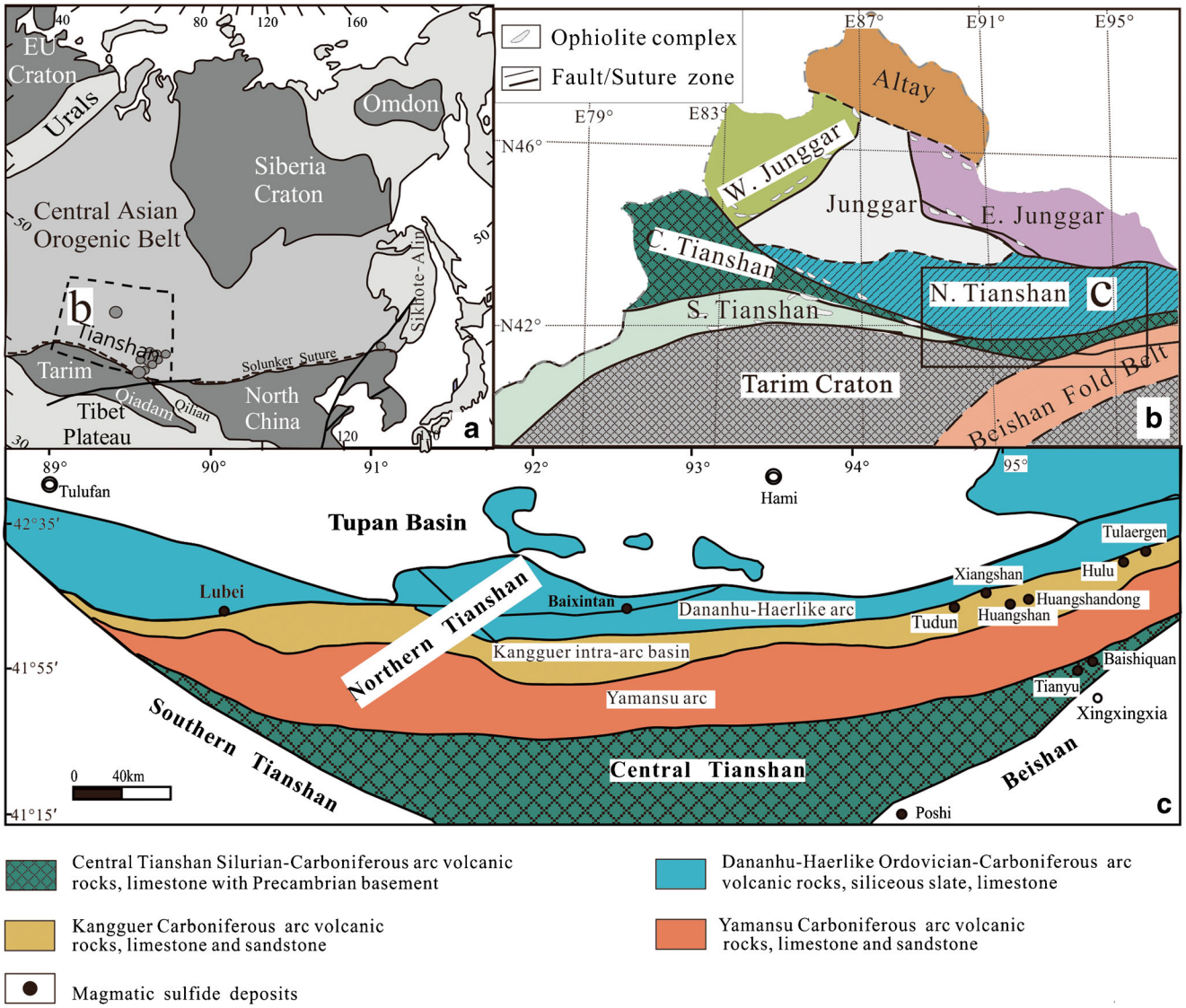

Fig. 1 **a** Schematic geological map of the Central Asian Orogenic Belt (modified after Jahn et al. 2000; Xiao et al. 2004). **b** Tectonic blocks of northern Xinjiang (after BGMX, 1993; Song and Li 2009; Song et al. 2013). **c** Simplified geological map of Northern Tianshan (after BGMX, 1993; Xiao et al. 2004; Song et al. 2011; Wang et al. 2015)

crystallization and magma mixing are also thought to have played some role in triggering S saturation during magma evolution in some deposits (Tang et al. 2012; Gao et al. 2013; Sun et al. 2013; Mao et al. 2015; Zhao et al. 2015).

Recent mapping, drilling, and geophysical survey in the western part of the Northern Tianshan have led to the discovery of the Baixintan and Lubei Ni-Cu sulfide occurrences (Li et al. 2014; Yang et al. 2017). The Baixintan intrusion is thought to have formed in a Permian post-orogenic setting, similar to intrusions in the eastern part of the Northern Tianshan (Wang et al. 2015, 2016a, b; Feng et al. 2017). The Permian Lubei mafic-ultramafic intrusions were formed from tholeiitic basaltic magmas derived from decompression partial melting of the metasomatized mantle in a post-collision extensional tectonic setting (Chen et al. 2018). However, it is unclear whether or not the mantle source and the sulfide saturation history of the Baixintan and Lubei intrusions are similar to those in the east. Here, we present new petrological, mineralogical, and geochemical data to constrain magma evolution and sulfide saturation processes of the intrusions in the western part of the Northern Tianshan.

Geological background

The CAOB is one of the largest accretionary orogens worldwide and comprises a complex collage of continental fragments, island arc assemblages, remnants of oceanic crust, and continental margins, set between the Siberian Craton to the north and the Tarim-North China Craton to the south (Fig. 1a; Sengör et al. 1993; Windley et al. 2007). The southern part of the CAOB in the northern Xinjiang consists, from north to south, of the Chinese Altai, the Junggar and Tianshan terranes, and the Beishan Fold Belt (Fig. 1b). The Tianshan terrane can be further divided into the Northern, Central, and Southern Tianshan (Fig. 1c; BGMX 1993; Xiao et al. 2004).

The Northern Tianshan is separated from the Central Tianshan by the Aqikkuduk fault and comprises, from north to south, the Bogda intra-arc basin, the Dananhu-Harlik island arc, and the Kanggur-Yamansu intra-arc basin (Ma et al. 1993; Jahn et al. 2000; Qin et al. 2002; Xiao et al. 2004, 2008; Fig. 1c). The Bogda intra-arc basin consists of Carboniferous bimodal volcanic rocks, marine carbonates, and epicontinental detrital rocks, as well as Permian bimodal volcanic rocks, conglomerates, and sandstones. The Late Carboniferous pillow basalts and high-alumina basalts are believed to have formed in a back-arc extensional environment (Xie et al. 2016a, 2016b), whereas the Permian bimodal volcanism in the southern Bogda zone may occur in a post-collisional tectonic setting, triggered by slab break-off (Shu et al. 2010; Chen et al. 2011). The Kanggur-Yamansu intra-arc basin contains the Shaerdelan Mesoproterozoic metamorphic core complex and Early Carboniferous submarine lavas, turbidites, pyroclastic rocks, basalt flows, andesitic tuffs, and tuffaceous sandstones (BGMX 1993; Xiao et al. 2004; Su et al. 2008; Zhou et al. 2010; Zhang et al. 2014). Mylonitized granites from the Shaerdelan metamorphic core complex have a zircon LA-ICP-MS U-Pb age of 921.7 ± 8.1 Ma (Su et al. 2008). Native copper-bearing basalts (307–318 Ma) within the Kanggur-Yamansu intra-arc basin have been interpreted to be derived from mafic magmatism generated through lithospheric delamination (Yuan et al. 2007; Zhang et al. 2013). More than 30 Early Permian mafic-ultramafic intrusions have been identified along the east-trending Kanggurtag fault, eight of which are known to host magmatic Ni-Cu sulfide deposits (Fig. 1c; Mao et al. 2008; San et al. 2010; Han et al. 2010; Song et al. 2013; Wang et al. 2015).

The Dananhu-Harlik arc is composed of Ordovician–Carboniferous tholeiitic basalt, calc-alkaline andesite, and pyroclastic rocks (Qin et al. 2002; Li et al. 2006a). Zircon U-Pb dating of volcanic rocks from the Kalatage area in the Dananhu-Harlik arc indicates that these rocks contain Proterozoic-inherited zircons (Long et al. 2017). There are various types of ore deposits in the Kalatage area, including the Silurian Honghai volcanogenic massive sulfide deposit, the Middle Devonian Xierqu skarn deposit, and the Middle Devonian Yudai porphyry deposit (Mao et al. 2010, 2017b; Deng et al. 2016). Adakites in the Early Carboniferous Tuwu-Yandong and Fuxing porphyry Cu deposits in the Dananhu-Harlik arc may have formed by partial melting of subducted oceanic crust (Zhang et al. 2006; Wang et al. 2016a). Several Early Permian mafic-ultramafic intrusions occur along the Kangguer and Dacaotan faults, but Ni–Cu mineralization has only been recognized in the Baixintan and Lubei intrusions (Fig. 1c; Li et al. 2006b; Ren et al. 2013; Wang et al. 2015, 2016a, b; Feng et al. 2017; Yang et al. 2017; Chen et al. 2018).

Petrography and mineralization of the Baixintan and Lubei intrusions

Baixintan intrusion

The Baixintan intrusion is ~ 3.1 km long, 0.8 km wide, and 0~0.3 km thick, with an areal extent of about 2.1 km^2 (Fig. 2). It comprises an upper hornblende gabbro, a lower hornblende gabbro, and a middle mafic-ultramafic unit with olivine gabbro, lherzolite, and olivine websterite, all emplaced in Middle Ordovician dacite and volcanic tuff of the Qieganbulake Formation (Li et al. 2014; Wang et al. 2015; Feng et al. 2017; Zhao et al. 2018). Zhao et al. (2018) reported a LA-ICP-MS zircon U-Pb Concordia age of 287 ± 3 Ma for the olivine gabbro, which is consistent with a LA-ICP-MS zircon Concordia age of 285 Ma ± 1 Ma reported by Feng et al. (2017).

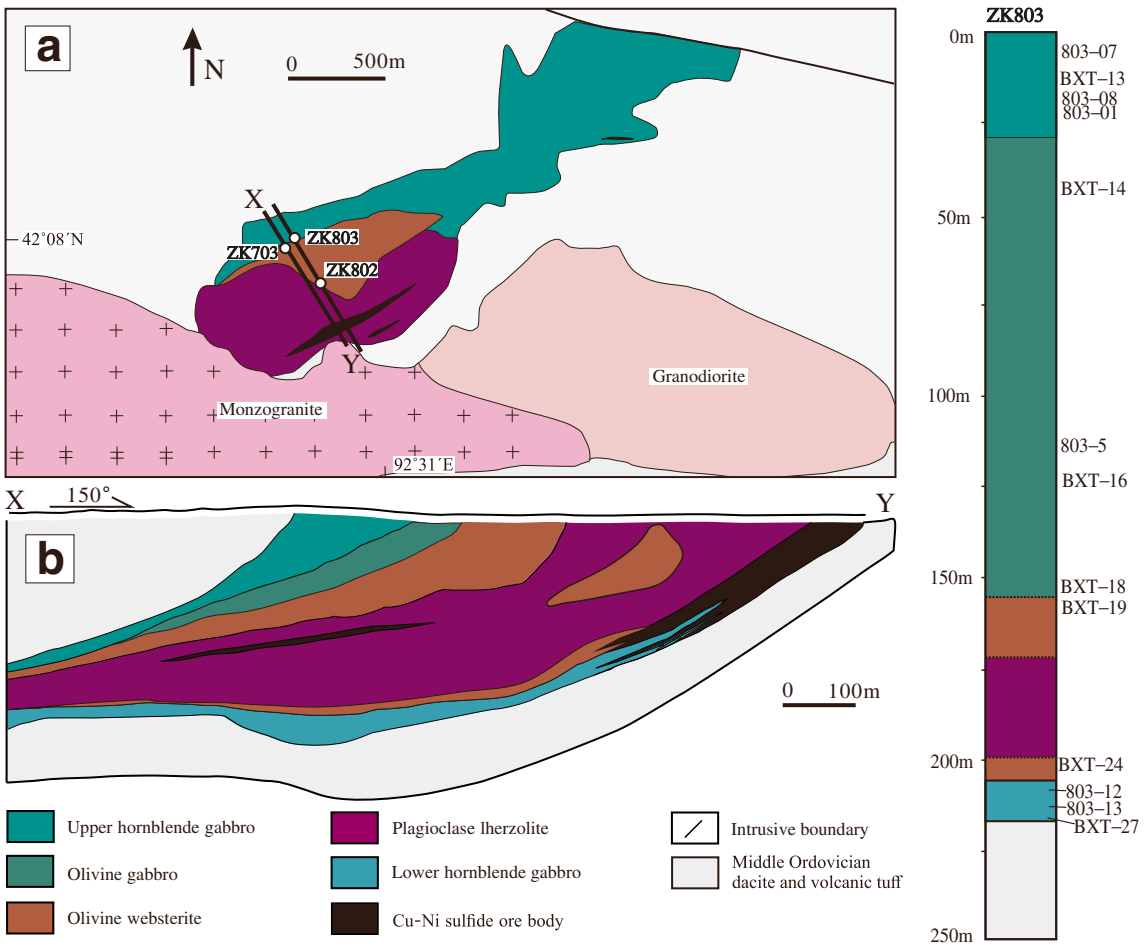

Fig. 2 **a**, **b** Simplified geological map and cross sections of the Baixintan intrusion (after Li et al. 2014; Wang et al. 2015)

The upper hornblende gabbro is cut by the olivine gabbro of the middle unit and in places is enclosed in olivine gabbro. The contacts between the olivine gabbro, lherzolite, and olivine websterite are generally gradational. The sharp contacts between the lherzolite of the middle unit and the lower hornblende gabbro indicate they formed from different magmatic pulses. The sulfides are mainly hosted in the lherzolite and lower hornblende gabbro with average grades of 0.46 wt% Ni and 1.02 wt% Cu (Li et al. 2014). The mineralization comprises pyrrhotite, pentlandite, chalcopyrite, and violarite.

The upper hornblende gabbro consists of coarse-grained plagioclase (60–65%), clinopyroxene (15–20%), hornblende (10–15%), and minor biotite (0–3%). In the middle unit, the olivine gabbro is composed of 15–20% olivine, 40–50% plagioclase, 5–10% orthopyroxene, 15–20% clinopyroxene, 5–10% hornblende, and 2% sulfide. Some plagioclase crystals are enclosed in olivine and clinopyroxene. The olivine websterite contains 20–35% olivine, 5–10% orthopyroxene, 10–35% clinopyroxene, 5–10% plagioclase, 5–8% hornblende, and 2–20% sulfide. The lherzolite contains 40–55% olivine, 3–5% orthopyroxene, 5–10% clinopyroxene, 5–10% plagioclase, 5–8% hornblende, and 2% sulfide. The olivine crystals are sub-rounded and enclosed in large orthopyroxene, clinopyroxene, plagioclase, and hornblende. The sulfides are commonly interstitial, but small, rounded sulfide inclusions also occur in some olivine crystals. The lower hornblende gabbro contains fine-grained plagioclase (60–70%), clinopyroxene (15–20%), hornblende (10–20%), and minor biotite (0–2%).

Lubei intrusion

The Lubei intrusion has an areal extent of about 0.36 km^2 (Fig. 3) and intrudes the Late Carboniferous andesite, dacite, and sandstone of the Xiaorequanzi Formation as well as the Late Carboniferous sandstones and limestones of the Gandun Formation. The intrusion comprises a lower hornblende gabbro overlain by olivine websterite and lherzolite. The contacts between lherzolite and olivine websterite are generally gradational. The lherzolite is crosscut by the lower hornblende gabbro. The sulfides are hosted in the lherzolite and lower hornblende gabbro with average grades of 0.64 wt% Ni and 0.48 wt% Cu (Yang et al. 2017). The mineralization comprises

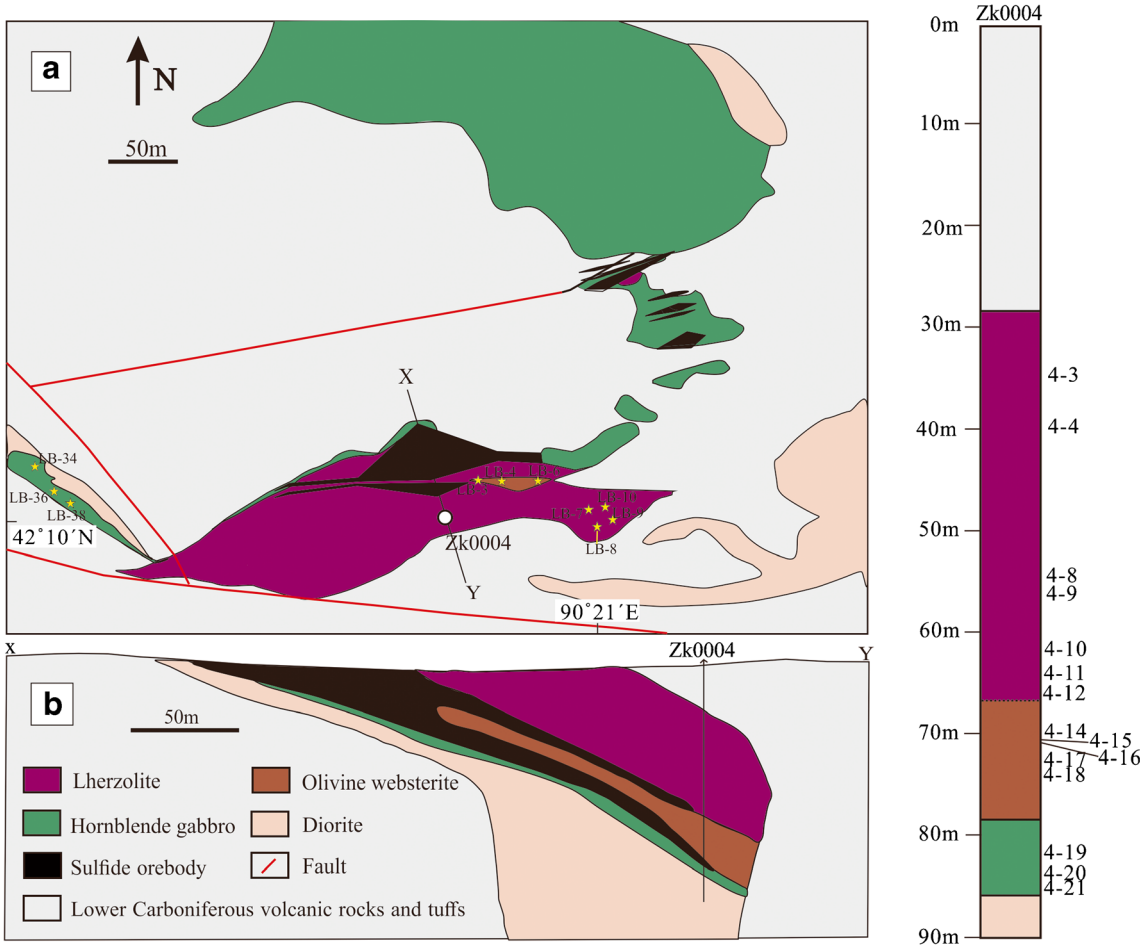

Fig. 3 **a**, **b** Simplified geological map and cross sections of the Lubei intrusion (after Yang et al. 2017)

pyrrhotite, pentlandite, and chalcopyrite with minor violarite. LA-MC-ICP-MS U-Pb zircon dating yielded a weighted mean age of 287.9 ± 1.6 Ma for the Lubei intrusion (Chen et al. 2018).

The lherzolite contains 50–65% olivine, 3–8% orthopyroxene, 5–10% clinoproxene, 2–15% plagioclase, 5–8% hornblende, and 2% sulfide. The sulfides are commonly interstitial, but small, rounded sulfide inclusions are also enclosed in olivine crystals. The olivine websterite contains 20–35% olivine, 5–10% orthopyroxene, 10–35% clinoproxene, 5–10% plagioclase, and 5–8% hornblende. Orthopyroxene is intergrown with clinopyroxene or enclosed in clinopyroxene and hornblende. The lower hornblende gabbro contains fine-grained plagioclase (60–70%), clinopyroxene (15–20%), and hornblende (10–20%).

Analytical methods

The samples from the Baixintan and Lubei intrusions were from weakly altered outcrops and drill core. The samples from the Baixintan intrusion included the upper hornblende gabbro, the olivine gabbro, lherzolite, olivine websterite, and the lower hornblende gabbro, whereas the samples collected from the Lubei intrusion included lower hornblende gabbro, olivine websterite, and lherzolite.

Zircon U-Pb geochronology

A gabbro sample (16LB-38) from the Lubei intrusion at 42° 9′ 41″ N and 90° 20′ 39″ E was selected for dating. The zircons for LA-ICP-MS U-Pb dating were processed by conventional magnetic and heavy liquid separation methods and then handpicked using a binocular microscope to select zircon grains for analysis. Approximately 30 kg of gabbro was crushed for zircon crystal separation. Sample preparation was carried out by the laboratory of the Regional Geological Mineral Survey Institute of Hebei Province, North China and 23 zircon crystals were recovered from the gabbro. The zircon grains were mounted on an epoxy resin disk and polished. Internal structure of the zircon grains was examined using cathodoluminescence (CL) before U-Pb isotopic analyses. The euhedral to subhedral zircons with striped absorption and oscillatory zoning rims in CL images were selected for

U-Pb LA-ICP-MS dating using an Agilent 7500a quadrupole mass spectrometer and GeoLasPro laser ablation system at the School of Resource and Environmental Engineering, Hefei University of Technology. The laser ablation system used a ComPex102ArF excimer laser (wavelength 193 nm) produced by Coherent Inc. of the USA. The standard zircon 91500 (Wiedenbeck et al. 1995) was used to correct for inter-element fractionation, and U, Th, and Pb concentrations were determined based on standard Mud Tank zircons (732 Ma; Black and Gulson 1978). Data processing was carried out using the Isoplot/Ex 2.49 programs of Ludwig (2001).

Zircon crystals from 16LBD-1 were separated using magnetic and density separation methods. Several clear, euhedral grains were isolated and pre-treated according to the chemical abrasion method of Mattinson (2005), with 60 h of annealing at 850 °C followed by 12 h of leaching in HF and HNO_3. Five single grains were selected and were cleaned with concentrated distilled HNO_3 and HCl. For ID-TIMS analysis, the samples were spiked with an in-house ^{205}Pb-^{235}U tracer solution, which has been calibrated against SRM 981, SRM 982 (for Pb), and CRM 115 (for U), as well as an externally calibrated U-Pb solution (the JMM solution from the EarthTime consortium). This tracer was regularly checked using "synthetic zircon" solutions that yield U-Pb ages of 500 and 2000 Ma, provided by D. Condon (BGS). Dissolution and equilibration of spiked single crystals were by vapor transfer of HF, using Teflon microcapsules in a Parr pressure vessel placed in a 200 °C oven for 6 days. Due to their small size, no chemical separation was required. The resulting residue was redissolved in HCl and H_3PO_4 and placed on an outgassed, zone-refined rhenium single filament with 5 μL of silicic acid gel. U-Pb isotope analyses were carried out at Curtin University, Perth, using a Thermo Triton Plus mass spectrometer, in peak-jumping mode using a secondary electron multiplier. Uranium was measured as an oxide (UO_2). Fractionation and dead time were monitored using SRM 981 and SRM 982. Mass fractionation was 0.02 ± 0.07%/amu. All uncertainties are reported at 2σ. Data were reduced and plotted using the software packages Tripoli (from CIRDLES.org) and Isoplot 4.15 (Ludwig 2012).

Mineral compositions

Olivines from the Baixintan and Lubei intrusive rocks were analyzed by wavelength-dispersive X-ray analysis using a Cameca SX100 electron microprobe at the Australian National University. The accelerating voltage was 15 kV, the beam current was 20 nA, and the counting time was set at 10 s. Standard Program International (SPI) mineral standards (USA) were used for calibration. Analytical results of natural mineral standards are presented in Appendix 1.

Major and trace elements

Samples were cut with a diamond-impregnated brass blade, crushed in a steel jaw crusher that was brushed and cleaned with de-ionized water between samples, and pulverized in an agate mortar in order to minimize potential contamination. They were analyzed using a PANalytical Axios X-ray fluorescence spectrometer (XRF) on fused glass beads at ALS Chemex (Guangzhou) Co. Ltd. with an analytical uncertainty less than 5%. Of powder, 0.7 g was mixed completely with $Li_2B_4O_7$-$LiBO_2$ flux and then fused to a glass bead at 1050~1100 °C in an automatic melting instrument. Analytical results of standard materials and replicate analyses are presented in Appendix 1.

Selected trace elements were determined using a PerkinElmer Sciex ELAN DRC-e ICP-MS at the Institute of Geochemistry, Chinese Academy of Sciences, with analytical uncertainty better than 10%. Samples were digested with 1 ml of HF and 0.5 ml of HNO_3 in screw top PTFE-lined stainless steel bombs at 190 °C for 12 h. The analytical precision is generally better than 1% for elements with concentrations > 200 ppm and 1–3% when less than 200 ppm. The procedure for the trace elements is described in detail by Qi et al. (2000). Reference standards GBPG-1, OU-6, and AMH-1 were used to monitor the trace element analyses (Appendix 1). The analytical uncertainty of this procedure is better than 5% for most elements.

Chalcophile elements

PGE were determined by ID-ICP-MS using an improved Carius tube technique (Qi et al. 2007) at the Institute of Geochemistry, Chinese Academy of Sciences, Guiyang. Five grams of powdered sample was digested with 40 ml aqua regia in a 75-ml Carius tube placed in a sealed, custom-made, high-pressure, water-filled autoclave. The solution was used to collect PGE by Te coprecipitation (Qi et al. 2004). The measured results of PGE for the reference standard WGB-1 agree well with recommended values reported by Govindaraju (1994). Analytical precision and accuracy are generally better than 10%, and the duplicate samples match each other very well (Appendix 1). PGEs of the blank are generally less than 1 ppb: Ir < 0.05 ppb, Ru < 0.05 ppb, Rh < 0.05 ppb, Pt < 0.05 ppb, and Pd < 0.5 ppb. Nickel, Cu, and Se of the samples containing 3 to 20 vol% sulfides were measured using Varian ICP735-ES inductively coupled plasma emission spectrometer and PerkinElmer Elan 9000 ICP-MS, respectively, at ALS Chemex (Guangzhou) Co. Ltd. Whole-rock S contents were measured at ALS Chemex (Guangzhou) Co. Ltd. with the detection limits ~ 0.01 wt%. The samples were analyzed for total sulfur using a Leco furnace. The sample (0.01 to 0.1 g) was heated to approximately 1350 °C in an induction furnace while passing a stream of oxygen through the sample. Sulfur

dioxide released from the sample was measured by an IR detection system. The analytical precisions are ~8% for S, ~3% for Ni and Cu, and ~10% for Se.

Sr-Nd-Hf-S isotopes

For radiogenic isotope analysis, approximately 120 mg of powdered sample was placed in Teflon beakers with a HF + HNO_3 mixture and then heated on a hotplate at about 120 °C for 1 week. Strontium and Nd were then separated and purified by conventional cation-exchange techniques. The isotopic compositions of purified Sr and Nd solutions were measured on a TRITON thermal ionization magnetic sector mass spectrometer (TIMS) at the Institute of Geochemistry, Chinese Academy of Sciences, using the procedure described by Yang et al. (2010). Mass fractionation corrections for Sr and Nd isotopic ratios were based on the values of $^{86}Sr/^{88}Sr = 0.1194$ and $^{146}Nd/^{144}Nd = 0.7219$. The $^{87}Sr/^{86}Sr$ ratios of the NBS-987 Sr isotopic standards and $^{143}Nd/^{144}Nd$ ratios of the BCR-2 Nd isotopic standards determined during this study were 0.710255 ± 10 (2σ) and 0.512550 ± 8 (2σ). Detailed sample preparation and analytical procedures followed Zhang et al. (2001).

Hafnium isotopic compositions were measured over three analytical sessions using a ThermoFinnigan Neptune MC-ICP-MS coupled to an ArF excimer laser (193 nm) and fitted with a fast response two-volume He atmosphere HelEx ablation cell at the Australian National University (Eggins et al. 2005). The analytical conditions followed those described by Hiess et al. (2009).

Whole-rock sulfur isotopes of sulfides were measured on a Finnigan MAT 252 continuous flow isotope ratio mass spectrometry at the Institute of Geochemistry, Chinese Academy of Sciences, with an analytical uncertainty less than 0.2‰ (Appendix 1). Analyses of the GBW04414 S standard yielded a value of − 0.063‰ ($n = 12$). All sulfur isotopic data are reported relative to V-CDT in standard δ notation.

Results

Zircon U-Pb geochronology

The results of LA-ICP-MS U-Pb zircon analyses are listed in Appendix 2 and the U-Pb concordia diagrams are shown in Fig. 4. The zircons have U concentrations of 327–8379 ppm with Th/U ratios of 1.22–2.52. Analyses of the 23 individual zircons yield a concordant age of 277.8 ± 3.4 Ma with a mean square of weighted deviations (MSWD) of 0.42 (Fig. 4) indicating that the gabbro from the Lubei intrusion was formed in the Early Permian.

ID-TIMS U–Pb data of the zircons in the lherzolite (16LBD-1) from the Lubei intrusion are listed in Appendix 3. Analyses of three of the five individual zircon crystals form a single concordant group and yield a weighted mean $^{206}U/^{238}Pb$ age of 279.7 ± 0.2 Ma with a MSWD of 0.30 (Fig. 4c). Uranium concentrations were between 100 and 200 ppm, with Th/U ratios between 0.5 and 1.0. Two older

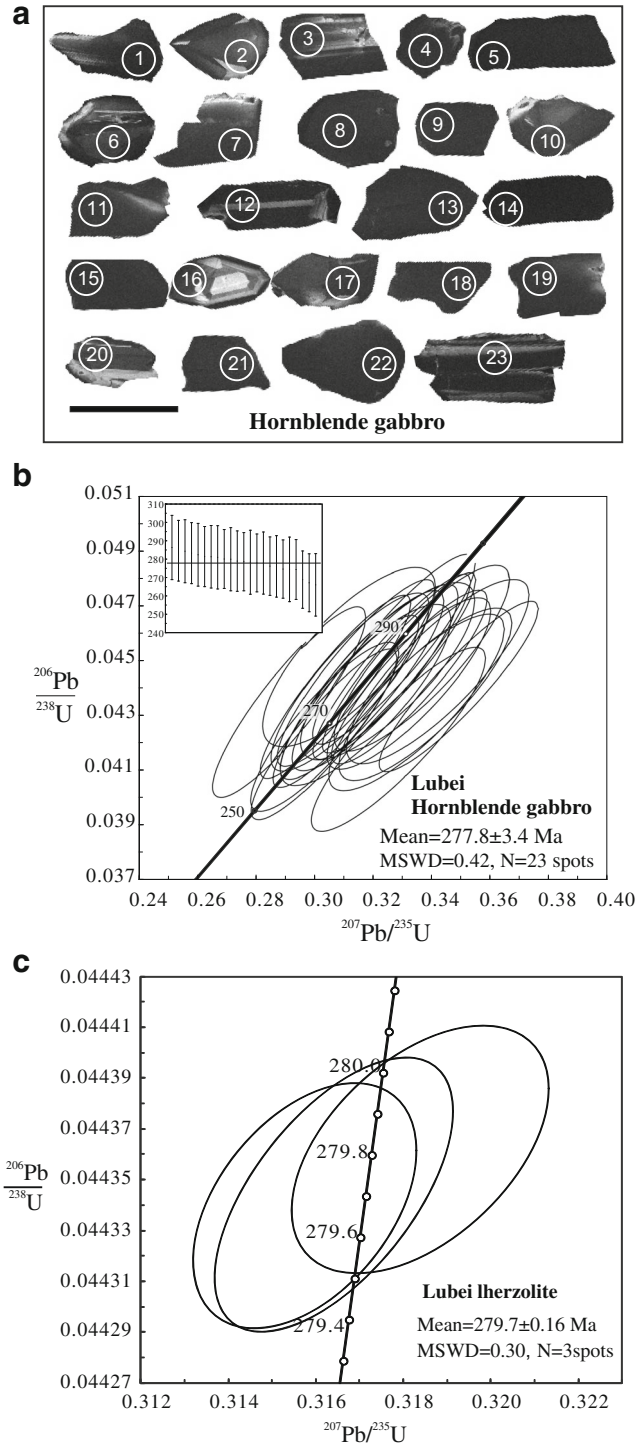

Fig. 4 **a**, **b** CL images and Concordia plot of LA-ICP-MS U-Pb analyses of zircons from the hornblende gabbro in the Lubei intrusion. **c** Concordia plots of ID-TIMS zircon U-Pb geochronological results for the Lubei lherzolite

zircons, at 325 and 431 Ma, are considered to be xenocrysts. The crystallization age of the lherzolite is identical to the gabbro of the Lubei intrusion within analytical uncertainties.

Mineral compositions

Olivine grains were analyzed from the lherzolite and olivine websterite of the Baixintan and Lubei intrusions (Appendices 4 and 5). The olivine crystals in all these samples have low Ca contents (< 1214 ppm; Appendices 4 and 5). The olivines of the lherzolite in the Baixintan intrusion have forsterite (Fo) values varying from 83.0% to 85.2% and Ni from 1486 to 1838 ppm, whereas the olivines of the lherzolite in the Lubei intrusion have higher Fo (84.5–85.8) and Ni contents of 1550 to 2089 ppm.

Major and trace element geochemistry

Representative major and trace element analyses of the Baixintan and Lubei intrusions are provided in Appendices 6 and 7. The lherzolite of the Baixintan intrusion contains the highest MgO (27.1–27.5 wt%) and $(Fe_2O_3)_T$ (12.1–12.5 wt%) and lowest SiO_2 (42.3–43.7 wt%) and CaO (3.92–4.40 wt%; Appendix 6). The olivine websterite has lower MgO (20.0–20.3 wt%) and $(Fe_2O_3)_T$ (10.2–10.7 wt%) contents and higher SiO_2 (44.1–44.8 wt%) and CaO contents (5.79–5.98 wt%) than the lherzolite. The olivine gabbro has higher MgO (13.6–18.9 wt%) but lower SiO_2 (44.3–45.1 wt%) and CaO contents (6.44–8.87 wt%) than those of the upper and lower hornblende gabbros.

The lherzolite of the Lubei intrusion contains 28.9–33.0 wt% MgO and 38.3–41.2 wt% SiO_2. With decreasing MgO, $(Fe_2O_3)_T$ decreases from 14.5 to 12.3 wt% and CaO and Al_2O_3 increase from 2.01 and 3.30 to 2.90 and 5.72 wt%, respectively (Appendix 7). The olivine websterite has lower MgO (24.1–28.4 wt%) and higher Al_2O_3 and CaO contents (2.09–11.0 wt% and 1.06–7.40 wt%, respectively) than the lherzolite. The hornblende gabbro has the lowest MgO (4.01–15.0 wt%) and highest SiO_2, Al_2O_3, and CaO contents (41.6–49.3, 10.8–17.0, and 2.96–3.42 wt%) of all the samples analyzed.

Normal Mid-Ocean Ridge Basalt (N-MORB) normalized trace element diagrams show that the Baixintan and Lubei intrusive rocks are enriched in large ion lithophile elements (e.g., Rb, Th, U, and La) relative to the high field strength elements (e.g., Zr, Hf, and Yb) which exhibit negative Nb-Ta-Ti anomalies. The Baixintan intrusive rocks contain higher trace element contents than those of the Lubei intrusion (Fig. 5). Except for the olivine websterite of the Lubei intrusion, all the intrusive rocks show positive Sr anomalies. The Baixintan and Lubei rocks are uniformly enriched in LREE relative to HREE ($(La/Yb)_N = 1.56–6.86$) and have variable Eu anomalies ($\delta Eu = 0.66–1.29$; Fig. 5).

Chalcophile element geochemistry and S isotopes

The concentrations of PGE, Cu, Ni, S, and Se in the ultramafic rocks and sulfides are presented in Appendix 8. Sulfide contents in the sulfide-mineralized samples were calculated using the procedure of Barnes and Lightfoot (2005): $C_{(100\%sul)} = C_{wr} \times 100 / (2.527 \times S + 0.3408 \times Cu + 0.4715 \times Ni)$. $C_{(100\%sul)}$ is the concentration of Pd or Pt in 100% sulfide; C_{wr} is the concentration of the element in the whole rock; and S, Cu, and Ni are the concentrations in weight percent of those elements in the whole rock. The ΣPGE abundances in the Baixintan intrusive rocks range from 1.87 to 4.41 ppb, which are lower than in the Lubei intrusion (4.06 to 44.3 ppb). The sulfide-bearing intrusive rocks of the Baixintan intrusion have lower ΣPGE content (6.63–20.6 ppb) than in the Lubei intrusion (9.12–213 ppb; Fig. 6). Copper/Pd ratios of the silicate rocks are between 4.76×10^4 and 2.57×10^5, much higher than primitive mantle values (7000–10,000; Barnes and Maier 1999), except one sample (LB-7) which has a Cu/Pd ratio of 8076. The mantle-normalized patterns of Ni, Cu, and PGE, for the intrusive rocks, are PGE depleted relative to Ni and Cu and show PPGE (Pt, Pd, and Rh) enrichments relative to IPGE (Ir, Ru; Fig. 7). The Se/S ratios of the sulfides in the Baixintan and Lubei intrusions range from 181×10^{-6} to 418×10^{-6}, with the majority close to the mantle ratios ($230–350 \times 10^{-6}$; Eckstrand et al. 1989). The $\delta^{34}S_{CDT}$ values of the sulfides from the Baixintan and Lubei intrusions are low, varying between −0.13‰ and 0.90‰ (Appendix 8), similar to typical mantle values (0 ± 2‰; Ohmoto and Rye 1979) but different from those of the country rocks (− 8.50‰ in Bainxintan area and 6.52‰ in Lubei area).

Sr-Nd-Hf isotopes

Strontium and Nd isotope data for the Baixintan and Lubei intrusions are calculated to have an initial age of 287 and 278 Ma, respectively (Appendix 9; Zhao et al. 2018). The Baixintan intrusive rocks have low initial $(^{87}Sr/^{86}Sr)_t$ ratios (0.70354–0.70628) and high $\varepsilon Nd_{(t)}$ (4.88–7.05), whereas the Lubei intrusive rocks have variable initial $(^{87}Sr/^{86}Sr)_t$ ratios (0.70400–0.70713) and $\varepsilon Nd_{(t)}$ (2.80–6.32; Fig. 8). The Hf isotopes of zircon crystals from Baixintan and Lubei intrusion determined by in situ LA-MC-ICP-MS are listed in Appendix 10. The εHf ($t = 287$ Ma) values of the Baixintan zircons range from 2.5 to 18.4 and the Lubei from 3.18 to 16.1.

Discussion

Our new zircon U-Pb ages of the lherzolite and hornblende gabbro suggest the Lubei intrusion was emplaced in the Early Permian. The ages of the Baixintan and Lubei intrusions indicate they are contemporary with other known major

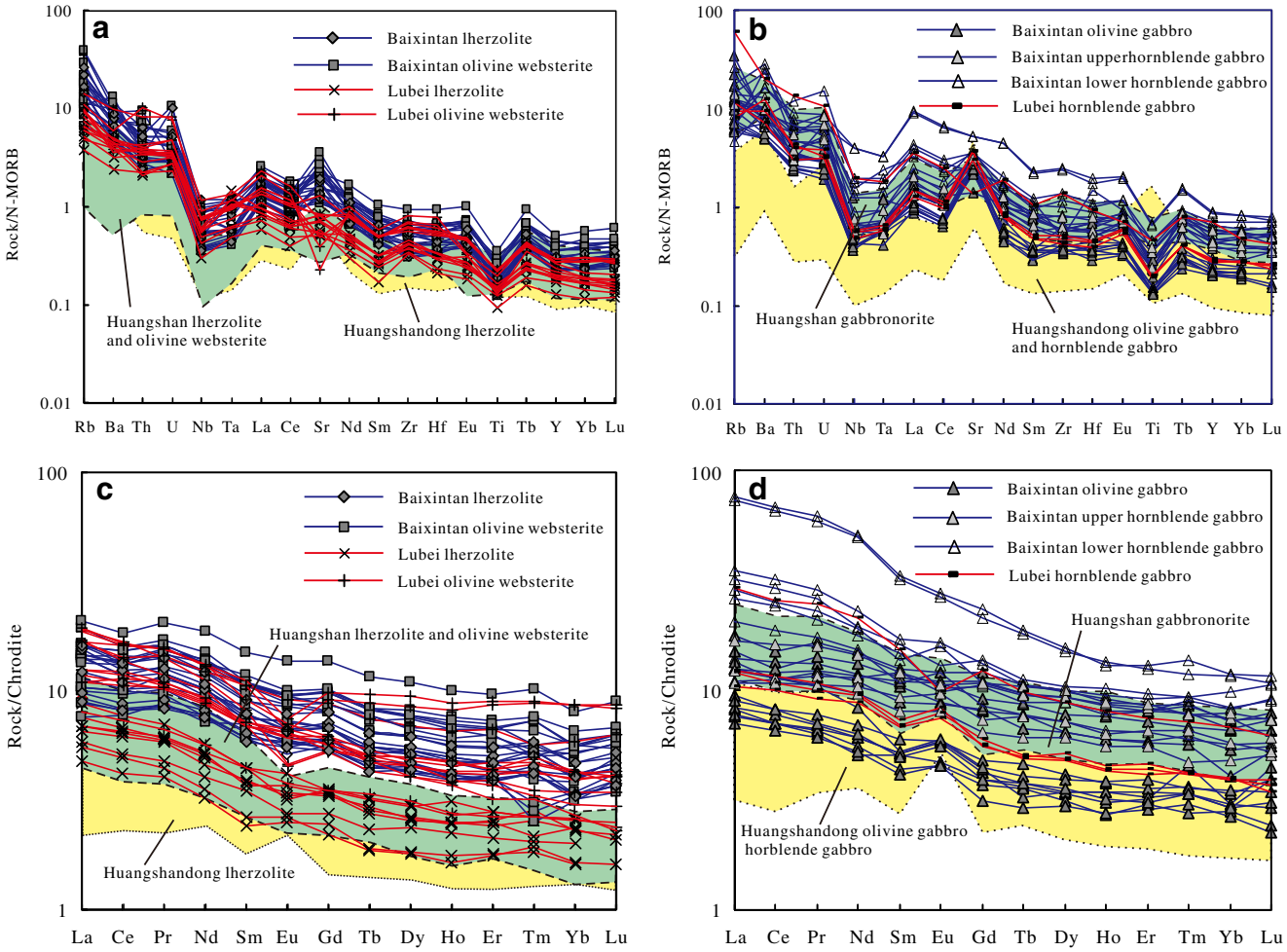

Fig. 5 **a**–**d** N-MORB normalized trace element spider diagrams and chondrite-normalized REE patterns for intrusive rocks in the Baixintan and Lubei intrusions. The data for the Huangshan and Huangshandong intrusions is from Deng et al. (2011a, b, 2014, 2015, 2017). Additional data for Baixintan intrusion is from Zhao et al. (2018) and Wang et al. (2015). N-MORB normalization and REE chondrite values are from Pearce (1982) and Sun and McDonough (1989), respectively

magmatic Ni-Cu sulfide deposits in the Northern Tianshan (Qin et al. 2011; Zhao et al. 2018; Feng et al. 2018; Chen et al. 2018). The Baixintan and Lubei intrusions are characterized by enrichment of Rb, Ba, U, and Sr, in conjunction with depletions of Nb, Ta, and Ti relative to N-MORB, which is similar to the other Ni-Cu sulfide-bearing intrusions in the Northern Tianshan. However, the $\varepsilon Nd_{(t)}$ values of the Baixintan and Lubei intrusive rocks are lower than those of the Huangshan and Huangshandong intrusive rocks, and the $\varepsilon Hf_{(t)}$ valuables are more variable (Fig. 8; Su et al. 2012; Sun et al. 2013). The Cu and PGE contents of the sulfides and intrusive rocks in the Baixintan and Lubei intrusions are higher than those of the Huangshan and Huangshandong intrusions (Figs. 6 and 7). The olivine from the lherzolites in the Baixintan intrusion contains higher Ni content than those of the latter. This suggests that the Baixintan and Lubei rocks in the west of the Northern Tianshan underwent a different magma evolution process than the rocks from the Huangshan and Huangshandong intrusions in the east.

Nature of the mantle source

The samples from the Baixintan and Lubei intrusions are enriched in large ion lithophile element and depleted in Nb, Ta, and Ti relative to N-MORB. The depletion in high field strength elements (such as Nb, Ta, and Ti) is normally interpreted to reflect magma generation in a subduction-related environment (Pearce 1983; Hawkesworth et al. 1997; Johnson and Plank 1999) or addition of relatively old continental crust (Wilson 1989). The similar bulk solid/melt partition coefficient of Nb, U, and La (Hofmann 1988; Sun and McDonough 1989) means that they will not be significantly fractionated during magma crystallization processes, and consequently, the Nb/U and La/Nb ratios of the intrusive rocks can be compared with the volcanic rocks to trace the ratios in the mantle source or crustal contamination process. Compared with average crust, N-MORB, ocean island basalt (OIB), and primitive mantle, the Baixintan and Lubei intrusions have lower Nb/U ratio and higher La/Nb ratios, respectively

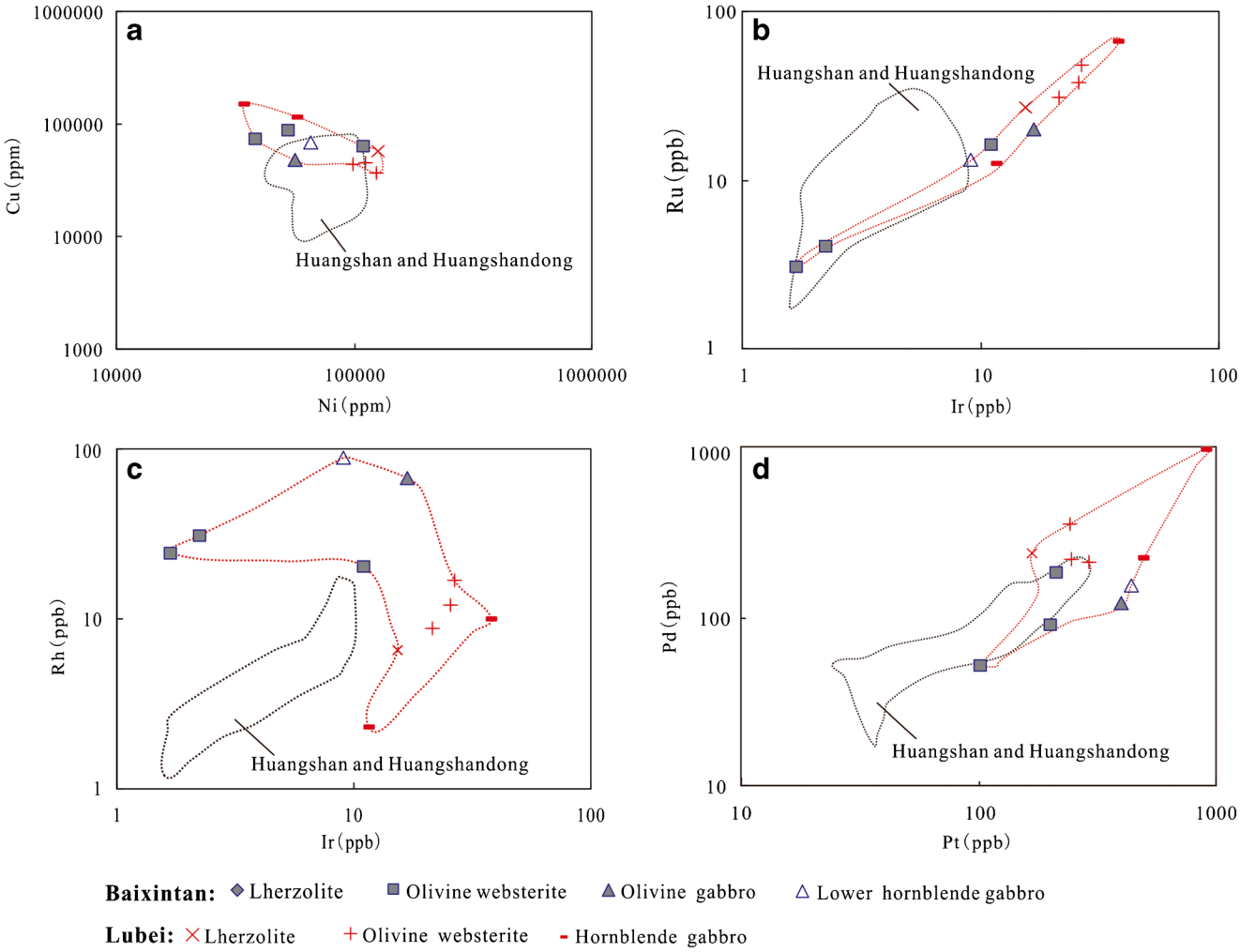

Fig. 6 **a**–**d** Plots of platinum group elements of the sulfides from the Baixintan and Lubei intrusions on a 100% sulfide basis. The data for the Huangshan and Huangshandong intrusions is from Deng et al. (2014, 2017)

(Appendix 11). Consequently, these trace elements ratios cannot be formed by the contamination of the mantle end-member with the crust but reflect the features of the mantle source of the intrusions. The Nb/U and La/Nb ratios of the Baixintan and Lubei intrusive rocks are similar to Alaskan-type intrusions (Pettigrew and Hattori 2006), suggesting that the primary magma of the intrusions was derived from a metasomatized mantle source.

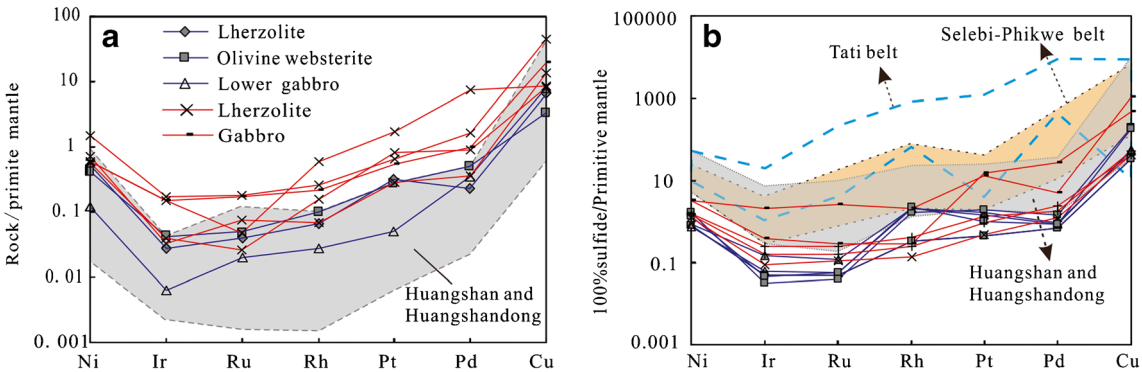

Fig. 7 **a**, **b** PGE patterns of intrusive rocks from the Baixintan and Lubei intrusions normalized to primitive mantle (Barnes and Maier 1999). Data for the Huangshan and Huangshandong intrusive rocks is from Deng et al. (2014, 2017). Also shown are fields for sulfide ores from the Tati and Selebi-Phikwe belts of eastern Botswana (Maier et al. 2008)

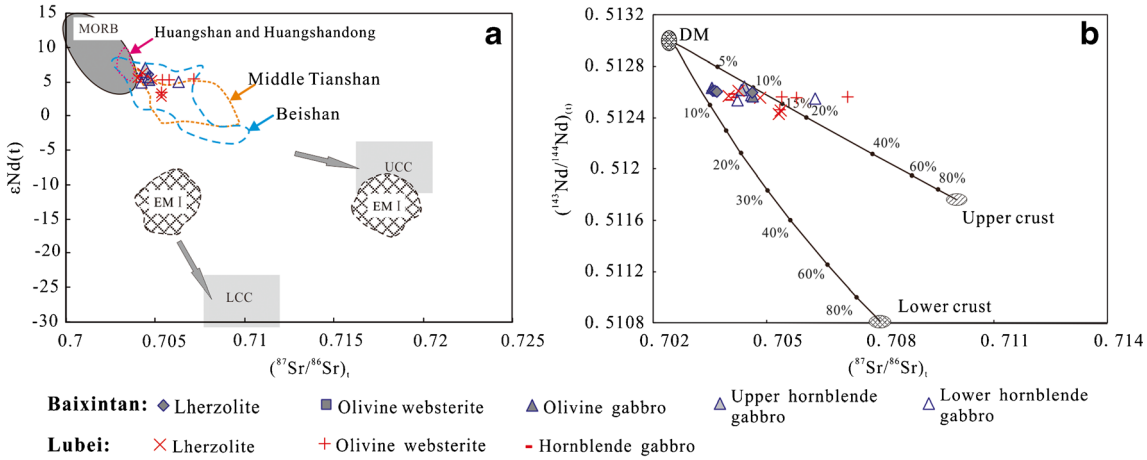

Fig. 8 Plot of **a** $\varepsilon Nd_{(t)}$ versus $(^{87}Sr/^{86}Sr)_t$. **b** Modeling calculations of Sr-Nd isotopes of the Baixintan and Lubei intrusions. Additional data from the Baixintan intrusive rocks is from Zhao et al. (2018). Data for the Central Tianshan and Beishan intrusions are from Sun et al. (2013). The fields for depleted MORB mantle, upper continental crust (UCC), and lower continental crust (LCC) are from Zindler and Hart (1986), Rudnick and Gao (2003), and Windrim and McCulloch (1986), respectively

Sulfur saturation

Previous studies have proposed that a metasomatized mantle source may experience high degree melting at a relative low temperature and generate the Ni-rich basaltic magmas which will form Ni-Cu sulfide deposits (Song and Li 2009; Ripley 2009). The primary magma of the Permian mafic-ultramafic intrusions from the western and eastern parts of the Northern Tianshan was derived from metasomatized mantle source (Zhang et al. 2011; Deng et al. 2014, 2015). Given the different scale of mineralization in the east and west, we explore what role the sulfide saturation mechanism played in generating the mineralization in the Northern Tianshan.

The Baixintan and Lubei intrusive rocks are characterized by variable initial $(^{87}Sr/^{86}Sr)_t$ ratios (0.70354–0.70713) and $\varepsilon Nd_{(t)}$ (2.80–7.05) and define a trend towards the upper crust (Fig. 8a). The isotopic variation suggests an upper crustal contamination either in the mantle source or during magma ascent. As the Precambrian crystalline basement of the Central Tianshan has not been subducted beneath the Northern Tianshan, the $\varepsilon Nd_{(t)}$ values of the intrusive rocks cannot be inherited from the mantle source which was metasomatized by subducted crustal materials (Xiao et al. 2004). Modeled $(^{87}Sr/^{86}Sr)_t$ and $\varepsilon Nd_{(t)}$ values show that < 20% contamination with the upper crust can explain the isotopic variations of the most samples in the Baixintan and Lubei intrusion (Fig. 8b). Previous studies suggest there is no Precambrian basement in the Northern Tianshan. However, zircons from andesites in the Lubei area have yielded concordant U-Pb ages of 325 ± 6 Ma and contain five zircon xenocrysts with an apparent $^{206}Pb/^{238}U$ age of 1602~1870 Ma (our unpublished data), suggesting that Precambrian crystalline basement has been incorporated in the formation of the volcanic rocks. Furthermore, a Mesoproterozoic metamorphic core complex has been discovered in the western part of the Northern Tianshan (Su et al. 2008). Thus, we propose that the Mesoproterozoic metamorphic core complex may be the source of the crustal contamination. Additionally, all zircon $\varepsilon Hf_{(t)}$ values of the Baixintan and Lubei intrusions are positive, falling into the range between chondrite and depleted mantle evolution trend lines, consistent with a parental magma derived from a depleted source mantle. The $\varepsilon Hf_{(t)}$ values of the Baixintan and Lubei intrusive rocks indicate that they have assimilated Tianshan basement rocks (Fig. 9).

The role of crustal sulfur in magmatic Ni-Cu sulfides can be constrained using Se/S ratios and $\delta^{34}S_{CDT}$ (Eckstrand et al. 1989; Ripley et al. 2002; Maier et al. 2008). The Se/S ratios of the sulfides in the Baixintan and Lubei intrusions range from 181×10^{-6} to 418×10^{-6}, with the majority close to the mantle ratios rather than crustal ratios (Eckstrand et al. 1989). These values are higher than those of the Huangshan and Huangshandong sulfide ores, which were segregated from magma that has assimilated crustal sulfur (Fig. 10; Mao et al. 2002; Tang et al. 2012; Deng et al. 2014, 2017). The $\delta^{34}S_{CDT}$ values of the sulfides from the Baixintan and Lubei intrusions are low, varying between − 0.13‰ and 0.90‰, similar to typical mantle values (0 ± 2‰; Ohmoto and Rye 1979) and the sulfide ores from the Huangshan and Huangshandong deposits (− 0.8‰ to 2.8‰; Deng et al. 2014, 2017) but different from those of the country rocks (− 8.50‰ in Bainxintan area and 6.52 ‰ in Lubei area). The Se/S ratios and $\delta^{34}S_{CDT}$ values of the Baixintan and Lubei sulfides resemble those values of mantle-derived rocks but are distinct from the crustal values, suggesting crustal sulfur has not been incorporated in the parent magma (Ohmoto and Rye 1979; Eckstrand et al. 1989). Consequently, sulfide saturation was not caused by assimilation of crustal sulfur in the Baixintan and Lubei intrusions.

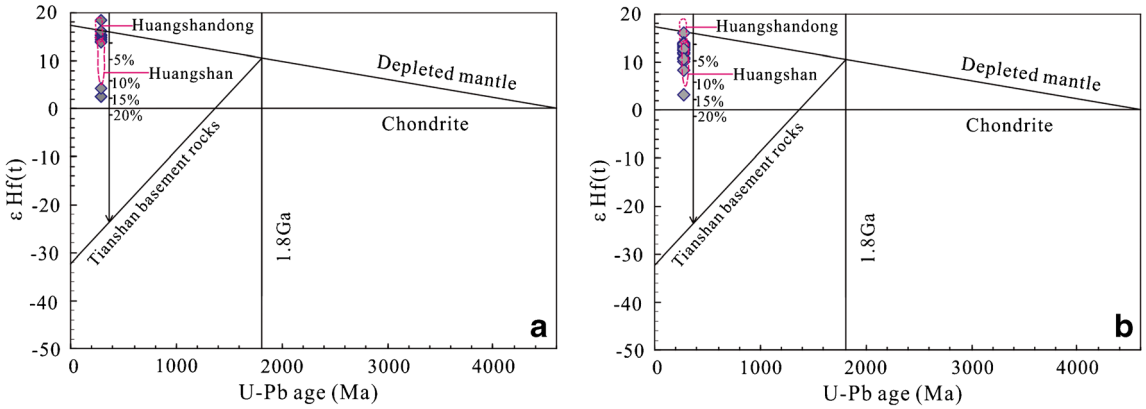

Fig. 9 **a**, **b** Plot of εHf versus U-Pb age of zircons of the Baixintan and Lubei intrusions. The age of the Tianshan basement rock is based on Hu et al. (2000). The concentration of Hf in N-MORB from Sun and McDonough (1989) is used to represent the composition of melt derived from depleted mantle. Data of the Huangshan and Huangshandong intrusions are from Su et al. (2013) and Sun et al. (2013). The numbers near the sample points are the degree of crustal contamination

A key question is what has driven the mafic magma to sulfide saturation in the Baixintan and Lubei intrusions. Because Pd/Zr are exceptionally sensitive to sulfide fractionation, they can be used to trace the segregation of even small amounts of magmatic sulfides from mafic magmas. Increasing $(Th/Nb)_{PM}$ (where PM = primitive mantle normalized) ratios are generally accepted to be the products of increasing degrees of crustal contamination (Lightfoot and Hawkesworth 1988; Keays and Lightfoot 2010). The similar bulk solid/melt partition coefficient of Nb and Th (Sun and McDonough 1989; Aldanmaz et al. 2000) means that they will not be significantly fractionated during magma crystallization processes, so Th/

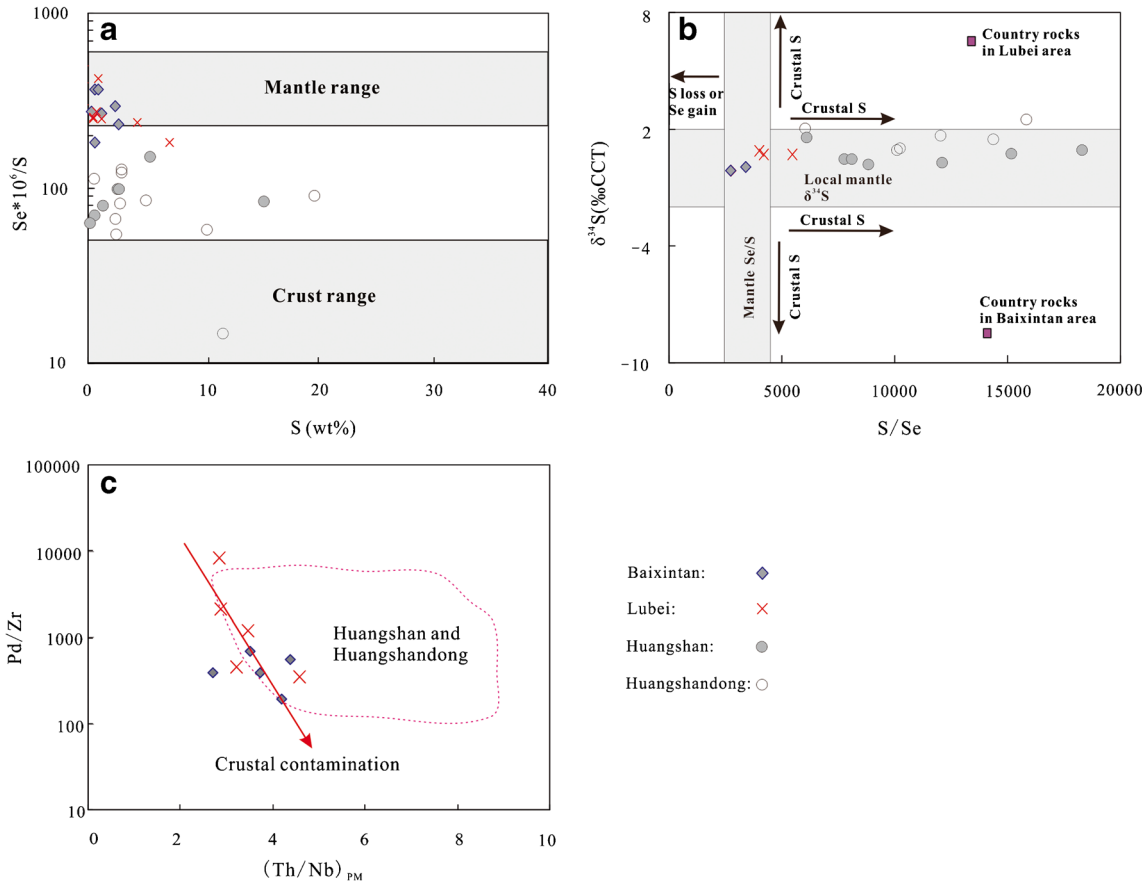

Fig. 10 Plots of **a** $Se*10^6/S$ versus S, **b** $Se*10^6/S$ versus $\delta^{34}S_{CDT}$, and **c** $(Th/Nb)_{PM}$ versus Pd/Zr for the Baixintan and Lubei mineralized rocks. Additional data for the Baixintan intrusion is from Zhao et al. (2018). The data for the Huangshan and Huangshandong ores are from Deng et al. (2014, 2017). The range in Se/S ratio of the mantle and crust is taken from Eckstrand et al. (1989)

Nb ratios of both intrusive and volcanic rocks can trace the crustal contamination process. The negative correlation between Pd/Zr and $(Th/Nb)_{PM}$ for the Baixintan and Lubei intrusive rocks suggests crustal contamination and chalcophile metal depletion (Fig. 10c). Crustal contamination would result in addition of SiO_2 and decreasing temperature which in turn could induce sulfide saturation by decreasing sulfur solubility (Lightfoot and Hawkesworth 1997; Li and Naldrett 2000; Seat et al. 2009). Experimental studies indicated that sulfur solubility of mafic magma decreases with decreasing Fe^{2+} content at a constant pressure (Wendlandt 1982; Mavrogenes and O'Neill 1999), so fractionation of mafic silicates may also play an important role in triggering sulfide saturation by sharply lowering the Fe concentration.

Origin of sulfide mineralization

Modeling of olivine compositional variations

As discussed above, Sr-Nd isotopic compositions indicate the Baixintan and Lubei intrusive rocks assimilated the lower crust in the Northern Tianshan, which would also have resulted in sulfide saturation (Lightfoot and Hawkesworth 1988; Keays and Lightfoot 2010). If crustal contamination has triggered extensive sulfide segregate in the lower crust, the sulfide would accumulate and form Ni-Cu sulfide mineralization whereas the residual metal-depleted magma would not form Ni-Cu sulfide deposits in the upper crust. On the other hand, if the crustal contamination only triggered trace sulfide saturation in the lower crust, the sulfide would extract some PGE from the magma and the residual PGE-depleted magma may form a Ni-Cu sulfide deposit in the shallow crust, as Ni and Cu would have been less depleted in the residual magma due to the lower partition coefficients in sulfide melt than that of PGE. Thus, it is necessary to investigate the sulfide segregation process to evaluate the exploration potential in the Baixintan and Lubei intrusions.

Because most of the lherzolites have poikilitic textures with abundant cumulate olivine and interstitial silicate minerals, we have used the method of Li and Ripley (2011) to estimate the parental magma composition of the Baixintan and Lubei intrusions. In our calculations, we used the average composition of sulfide-barren lherzolite samples containing the most primitive olivine (Fo = 85, Baixintan; Fo = 86, Lubei), the olivine-liquid exchange coefficient $(FeO/MgO)_{Ol}/(FeO/MgO)_{Liq}$ of 0.3 by Roeder and Emslie (1970), and an assumed $FeO/(FeO + Fe_2O_3)$ ratio of 0.95 and 0.98 for the liquid in the Baixintan and Lubei intrusions, respectively. The estimated MgO contents in the parental magma of Baixintan and Lubei intrusions are 7.90 and 7.79 wt%, respectively (Appendix 12).

Olivine chemistry is controlled by parental magma composition, fractional crystallization, sulfide segregation, subsolidus reequilibration with interstitial silicate, and trapped sulfide liquid; consequently, they are used as an indicator of magma evolution and sulfide saturation (Barnes 1986; Barnes et al. 2011, 2013; Li et al. 2001, 2007). We have used the PELE program (Boudreau and Meurer 1999) to investigate the fractional crystallization and sulfide segregation processes of the parental magma for the primitive lherzolite in the Baixintan and Lubei intrusions at 1 kb total pressure and a constant oxidation state equal to that of one log unit above the fayalite-magnetite-quartz buffer. The Rayleigh fractionation equation has been used to describe models for the Ni contents in olivine. In this paper, the partition coefficient of 7 was used for Ni between olivine and magma and 500 between sulfide liquid and magma (Li and Ripley 2005). The olivine Fo value and Ni content correlation curve A–B are the modeled result of normal magmatic evolution (Fig. 11). Curve A–C is the trend of olivine Fo value and Ni content when olivine and sulfide crystallized together. The observed Ni-Fo variations of olivine from the ultramafic rocks can be explained by olivine having crystallized from the silicate liquid that coexisted with the sulfide liquid (Fig. 11).

Although olivines from the lherzolite in the Baixintan and Lubei intrusions have similar Fo values to those of the Huangshan and Huangshandong intrusions, the Ni contents of most olivines in the Baixintan and Lubei (796–2664 ppm) are higher than those of the Huangshan and Huangshandong (282–1295 ppm; Fig. 11). What causes the Ni contents differences in olivines between the intrusions in the west part and east part of Northern Tianshan? Since samples containing > 0.5 wt% S were excluded, the differences in olivine composition did not result from postcrystallization reaction between olivine and sulfide. Similarly, because the olivine compositions of these intrusions do not plot along the modeled path of normal olivine crystallization, fractional crystallization cannot account for the variations of the Ni contents of olivines (Fig. 11). "Trapped silicate liquid shift" generally generates olivine with a composition that is poorer in Mg and Ni contents than the original material (Li and Ripley 2003; Li et al. 2007). The Baixintan and Lubei intrusions have similar Fo values of olivines to those of the Huangshan and Huangshandong intrusions, suggesting that the lower Ni contents in olivine compositions of the Huangshan and Huangshandong intrusions cannot be explained by subsolidus reequilibration with interstitial silicate liquid. The Ni contents of most primitive olivine in the Baixintan intrusion are high (up to 2664 ppm), similar to those of most primitive olivine from in the Huangshannan magmatic Ni-Cu ore deposit (~ 3300 ppm Ni in olivine, Mao et al. 2017a), and higher than that in Jinchuan and Noril'sk deposits (Li and Ripley 2003; Li et al. 2004). Our modeling yielded estimates of 400 and 220 ppm Ni for the parental magma from which the olivine crystallized in the Baixintan and Lubei intrusion, respectively. As noted above, the high Ni contents of olivine in the Baixintan and Lubei intrusions were not the result of fractional crystallization, sulfide segregation, and subsolidus

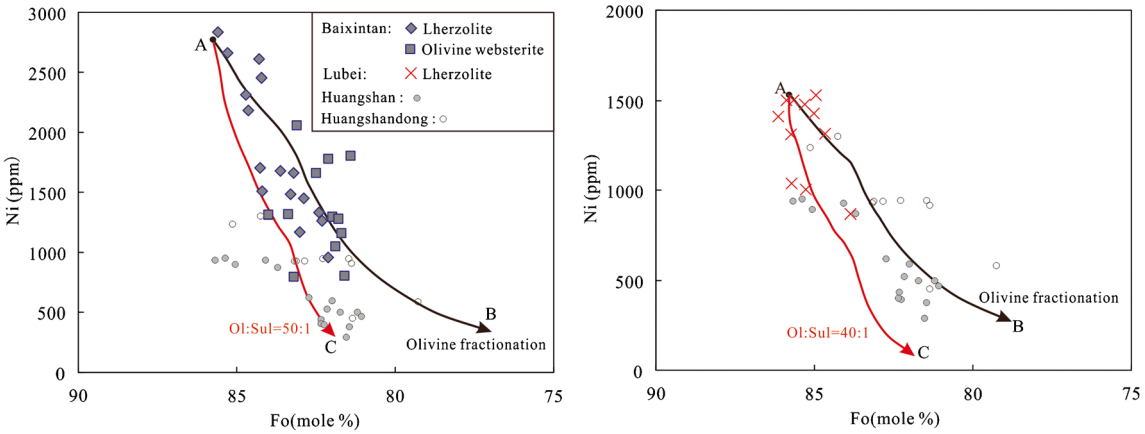

Fig. 11 Model calculation of the variation of nickel content and Fo of the olivine in the Baixintan intrusion (**a**) and Lubei intrusions (**b**). For detailed methodology, see Li and Naldrett (1999) and Li et al. (2007). The olivine compositions of the Huangshan and Huangshandong intrusions are from our unpublished data. A is the olivine composition in equilibrium with the parental magma. We use a partition coefficient of Ni between olivine and magma of 7 at 2.5 kbar and a FMQ + 1-equivalent oxidation state (Li and Ripley 2005). A and B are the calculated curve modeling of the olivine crystallization of the parental magma. A and C are the calculated curve modeling of olivine crystallization and sulfide segregation simultaneously

reequilibration; rather, they may have been the result of high Ni contents in the parent magmas.

Quantitative modeling of sulfide segregation

The parental magma of the Baixintan and Lubei intrusions had higher Ni contents than the Huangshan and Huangshandong intrusions. Consequently, we propose that crustal contamination in the Baixintan and Lubei intrusions would not have triggered extensive sulfide segregation in the lower crust. We investigate the sulfide segregation history of the Baixintan and Lubei intrusions by examining the composition of sulfides. Metal contents of sulfide melts segregated from silicate magma are a function of the R factors (ratio between silicate melt and sulfide liquid) and the metal partition coefficients (Campbell and Naldrett 1979):

$$C\text{sul } i = C\text{sil } i \times D_i \times (R+1)/(R+D_i) \quad (1)$$

where Csul i and Csil i represent the content of element i in the sulfide liquid and in the parental silicate liquid, respectively, D_i is the partition coefficient of element i between sulfide liquid and silicate liquid, and R is the R factor.

The geochemical signatures of the Baixintan and Lubei intrusions suggest that the parental magmas were derived from metasomatized mantle similar to those of island arc magmas. Consequently, we assume that the parent magma is similar to typical island arc basalt, with 7.5 ppb Pd and 400 ppm Ni (Barnes et al. 1993; Kelemen et al. 2004; Thakurta et al. 2008). The partition coefficients of Pd and Ni between sulfide and silicate magma were assumed to be 40,000 and 500, respectively (Peach et al. 1990; Fleet et al. 1993). The PGE modeling suggests that the source magma for the Baixintan and Lubei intrusions underwent two stages of sulfide segregation. First, the primary magma underwent 0.007% early sulfide removal at depth and lost much of its chalcophile content (Fig. 12). Then, sulfides in the Baixintan and Lubei intrusions were segregated from the strongly PGE-depleted parent magma under R factors of 100 to 800 in a shallow magma chamber.

The sulfide-bearing intrusive rocks of the Baixintan intrusion have lower ΣPGE contents (6.63–20.6 ppb) than those of the Lubei intrusion (9.12–213 ppb). The Cu and PGE contents

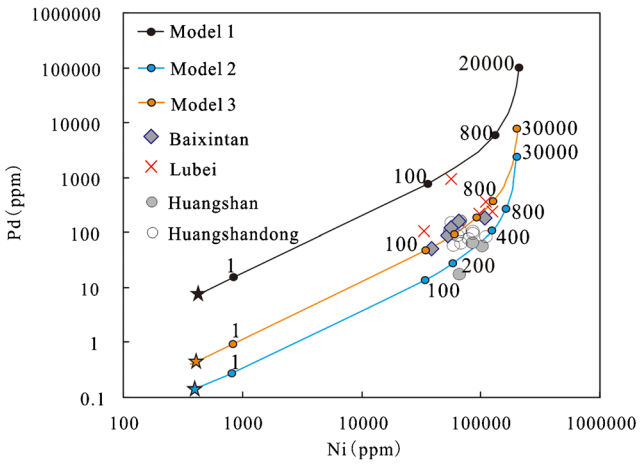

Fig. 12 Variations of metal tenors in the disseminated sulfide from the Baixintan and Lubei intrusions. The Pd and Ni concentrations of the sulfides are on a 100% sulfide basis. Model 1 presents the sulfide melts segregated from basaltic magma with 7.5 ppb Pd and 430 ppm Ni under variable R values (labeled in the diagram). Model 2 displays sulfide liquids separated from PGE-weakly depleted magma with 0.46 ppb Pd and 415 ppm Ni (because of 0.007% sulfide removal from magma) under different R values. Model 3 shows the sulfide liquids produced by sulfide immiscibility in a heavily PGE-depleted magma with 0.14 ppb Pd and 409 ppm Ni (because of 0.01% sulfide removal from magma). The PGE data of the Huangshan and Huangshandong sulfide ores are from Deng et al. (2014, 2017) and Mao et al. (2014, 2015)

of the sulfides in the Baixintan and Lubei intrusions are higher than those of the Huangshan and Huangshandong intrusions (Figs. 6, 7, and 12). The chalcophile element abundance of magmatic sulfides is controlled by some combination of the concentration of these elements in the parental silicate magma, the *R* factor, the degree of fractional crystallization of the sulfide liquid, and late hydrothermal alteration (Keays 1995; Barnes et al. 1997; Barnes and Lightfoot 2005). The ratios of Ir/(Ir + Ru) and Pt/(Pt + Pd) (0.36–0.48 and 0.41–0.82, respectively) of the Baixintan and Lubei intrusions are typical of magmatic sulfide (Naldrett et al. 1982), indicating that hydrothermal alteration has a limited effect on the PGE compositions of the sulfides in the Baixintan and Lubei intrusions. Commonly, the fractional crystallization of a sulfide liquid has a greater effect on the chalcophile element compositions of semi-massive and massive sulfides than those of disseminated sulfides (Naldrett 1994). As only disseminated sulfides were investigated, fractional crystallization of sulfides cannot have caused the variation in PGE contents. Moreover, the sulfides in the Baixintan and Lubei intrusions segregated from the magma under *R* factors of 100–800, similar to those of the Huangshan and Huangshandong intrusions (Sun et al. 2013; Deng et al. 2014, 2017; Mao et al. 2014, 2015), suggesting that the *R* factor did not cause the different PGE contents in sulfides. If more sulfides were removed from the primary magma, the residual magma would be more depleted in PGE. The sulfides segregated from this residual magma would have relatively low PGE contents (Fig. 12). Compared with the Baixintan and Lubei intrusions, the Huangshan and Huangshandong magmas may have experienced more sulfide removal at depth (Fig. 12; Gao et al. 2013; Sun et al. 2013; Deng et al. 2014, 2017). The early removal of sulfide in the Huangshan and Huangshandong intrusions would remove PGE from the magma, resulting in the residual magmas being more depleted in PGE than those in the Baixintan and Lubei intrusions. The more PGE-depleted residual magmas in the Huangshan and Huangshandong intrusions formed sulfide ores with lower PGE contents than those of the Baixintan and Lubei intrusions. In summary, the magmas of the Baixintan and Lubei intrusions were sulfide-saturated in the lower crust and a small amount of sulfides (~0.007%) was removed in staging chambers at depth. A second stage of sulfide saturation was reached in shallow magma chambers and formed the Ni-Cu sulfide mineralization.

Implications for Ni-Cu sulfide prospectivity

The most important factors required for the formation of a magmatic Ni-Cu sulfide deposit include (1) large amount of mantle-derived magma ascending into the crust, (2) the interaction of the source magma with country rocks to induce sulfide saturation, (3) the concentration of sulfides in conduits through which much magma has flowed, and (4) Ni-Cu upgrading of sulfide liquid by new, chalcophile-undepleted magma (Naldrett 1997, 1999; Li et al. 2000; Maier et al. 2001; Barnes and Lightfoot 2005). If any mafic-ultramafic intrusive rocks develop these geological features, they would have exploration potential for the magmatic Ni-Cu sulfide deposit.

The mafic-ultramafic intrusions in the western part of the Northern Tianshan formed in the early Permian (278–287 Ma; Fig. 4; Zhao et al. 2018; this study), coeval with the Ni-Cu sulfide-bearing intrusions in the eastern part of the Northern Tianshan. The trace element and isotopic composition of the Baixintan and Lubei intrusions suggest that the primary magmas were derived from metasomatized lithospheric mantle. Combined with the widespread Permian mafic-ultramafic intrusions in the western part of the Northern Tianshan, these intrusions are interpreted to be linked to large volumes of post- or syn-collisional tholeiitic magmatism induced by asthenospheric upwelling (Li et al. 2006b; Song et al. 2011, 2013; Gao et al. 2013; Sun et al. 2013; Mao et al. 2014, 2015; Deng et al. 2015, 2017; Feng et al. 2017). Secondary faults along the Huangshan-Kangguer fault likely provided zones of weakness along which magma ascended. Although no obvious crustal source of sulfur was incorporated into the magma, sulfide liquid saturation was achieved due to crustal contamination and fractional crystallization of mafic silicates and chromites. The modeling of PGE suggests that the sulfide liquids underwent upgrading of PGE and Ni by reaction with successive pulses of magma under *R* factors of 100–800 (Fig. 12). Moreover, the olivine compositions and chalcophile elements of mafic-ultramafic intrusions suggest that the parental magma of the intrusive rocks in the western part of the Northern Tianshan contains higher chalcophile elements than those of the eastern part. The Permian mafic-ultramafic intrusions in the west of the Northern Tianshan have a similar mantle source to the Huangshan and Huangshandong intrusions and experienced sulfide saturation and metal upgrading processes. Therefore, they should be regarded as favorable Ni-Cu sulfide exploration targets. All world-class magmatic Ni-Cu deposits have been contaminated by crustal sulfur to achieve sulfide saturation (Naldrett 1999; Keays and Lightfoot 2010; Ripley and Li 2013). Previous studies proposed that more than 50% sulfur in some magmatic Ni-Cu sulfide deposits are from country rocks (Kabanga, Maier and Barnes 2010; Noril'sk, Robertson et al. 2015). Compared to the Huangshan and Huangshandong intrusive rocks, the $\varepsilon Nd_{(t)}$ and the $\varepsilon Hf_{(t)}$ values of the Baixintan and Lubei intrusive rocks are relatively low, suggesting that Huangshan and Huangshandong rocks have assimilated more crustal material than the Baixintan and Lubei rocks (Fig. 8a). The Ni contents in the parental magma of the Baixintan and Lubei intrusions are higher than those of the Huangshan and Huangshandong deposits. As the

Baixintan and Lubei intrusions assimilated less crustal sulfur (Fig. 10), even though the volumes of basalt were similar, it is likely that the country rocks did not supply as much sulfur as the Huangshan and Huangshandong deposits. Consequently, the Baixintan and Lubei intrusions do not have the same Ni-Cu potential as the Huangshan and Huangshandong deposits.

Conclusions

Zircon U-Pb geochronology shows that the Lubei mafic-ultramafic intrusion formed at 278 Ma. The primary magma of the Baixintan and Lubei mafic-ultramafic intrusions was derived from metasomatized mantle. The Baixintan and Lubei intrusive rocks have assimilated Precambrian basement in the western Northern Tianshan. Sulfide saturation was triggered by crustal contamination and fractional crystallization rather than crustal S addition. The parental magma of the intrusive rocks in the Baixintan and Lubei intrusions contains higher chalcophile elements than those of the Huangshan and Huangshandong intrusions.

Acknowledgments This work was supported by the National Natural Science Foundation of China (Grant Nos. U1803113, 41672069, 41630316, 41303031, and 41820104007), the China Academy of Science "Light of West China" Program, and the Fundamental Research Funds for the Central Universities (JZ2018HGTB0246). We are very grateful to Weidong Li, Jiangtao Tian, and Dahai Li for the help during our field work. We also thank Kaiyuan Wang, Jing Hu, and Fang Xiao for their kind help on the analyses of isotopes and trace elements. Critical comments from Professor Chusi Li, another anonymous reviewer, and editorial inputs from guest editor Professor Marco Fiorentini are greatly appreciated.

References

Aldanmaz E, Pearce JA, Thirlwall MF, Mitchell JG (2000) Petrogenetic evolution of Late Cenozoic, post-collision volcanism in western Anatolia, Turkey. J Volcanol Geotherm Res 102:67–95

Barnes SJ (1986) The effect of trapped liquid crystallization on cumulus mineral compositions in layered intrusions. Contrib Mineral Petrol 93:524–531

Barnes SJ, Lightfoot PC (2005) Formation of magmatic nickel sulfide group ore deposits and processes affecting their copper and platinum-group element contents. Economic Geology 100th Anniversary Volume: 179–213

Barnes SJ, Maier WD (1999) The fractionation of Ni, Cu, and the noble metals in silicate and sulfide liquids. In Dynamic processes in magmatic ore deposits and their application to mineral exploration. In: Keays RR, Lesher CM, Lightfoot PC, Farrow CEG (eds) Geological Association of Canada, Short course notes 13, pp 69–106

Barnes SJ, Couture JF, Sawyer EW, Bouchaib C (1993) Nickel-copper occurrences in the Belleterre-Angliers belt of the Pontiac Subprovince and the use of Cu-Pd ratios in interpreting platinum-group element distributions. Econ Geol 88:1402–1419

Barnes SJ, Makovicky E, Makovicky M, Hansen JR, Moller SK (1997) Partition coefficients for Ni, Cu, Pd, Pt, Rh and Ir between monosulfide solid solution and sulfide liquid and the implication for the formation of compositionally zoned Ni–Cu sulfide bodies by fractional crystallization of sulfide liquid. Can J Earth Sci 34: 366–374

Barnes SJ, Osborne GA, Cook D, Barnes L, Maier WD, Godel B (2011) The Santa Rita nickel sulfide deposit in the Fazenda Mirabela intrusion, Bahia, Brazil: geology, sulfide geochemistry, and genesis. Econ Geol 106:1083–1110

Barnes SJ, Godel B, Gürer D, Brenan JM, Robertson J, Paterson D (2013) Sulfide-olivine Fe-Ni exchange and the origin of anomalously Ni rich magmatic sulfides. Economic Geology 108:1971–1982

BGMX (Bureau of Geology and Mineral Resources of Xinjiang Uygur Autonomous Region) (1993) Regional geology of Xinjiang Uygur autonomous region. Geological Publishing House, Beijing, pp 1–841 **(in Chinese with English abstract)**

Black LP, Gulson BL (1978) The age of the mud tank carbonatite, Strangways Range, Northern Territory. BMRJ J Aust Geol Geophys 3:227–232

Boudreau AE, Meurer WP (1999) Chromatographic separation of the platinum-group elements, gold, base metals and sulfur during degassing of a compacting and solidifying igneous crystal pile. Contrib Mineral Petrol 134:174–185

Campbell IH, Naldrett AJ (1979) The influence of silicate: sulfide ratios on the geochemistry of magmatic sulfides. Econ Geol 74:1503–1506

Chen XJ, Shu LS, Santosh M (2011) Late Paleozoic post-collisional magmatism in the Eastern Tianshan Belt, Northwest China: new insights from geochemistry, geochronology and petrology of bimodal volcanic rocks. Lithos 127:581–598

Chen BY, Yu JJ, Liu SJ (2018) Source characteristics and tectonic setting of mafic-ultramafic intrusions in Northern Xinjiang, NW China: insights from the petrology and geochemistry of the Lubei mafic-ultramafic intrusion. Lithos 308-309:329–345

Deng YF, Song XY, Jie W, Chen SL, Li J (2011a) Petrogenesis of the Huangshandong Ni-Cu sulfide-bearing mafic-ultramafic intrusion, Northern Tianshan, Xinjiang: evidence from major and trace elements and Sr-Nd isotope. Acta Geol Sin 85:1436–1451 **(in Chinese with English abstract)**

Deng YF, Song XY, Chen LM, Cheng SL, Zhang XL, Li J (2011b) Features of the mantle source of the Huangshanxi Ni-Cu sulfide-bearing mafic-ultramafic intrusion, eastern Tianshan. Acta Petrol Sin 27:3640–3652 **(in Chinese with English abstract)**

Deng YF, Song XY, Chen LM, Zhou TF, Pirajno F, Yuan F, Xie W, Zhang DY (2014) Geochemistry of the Huangshandong Ni-Cu deposit in northwestern China: implications for the formation of magmatic sulfide mineralization in orogenic belts. Ore Geol Rev 56:181–198

Deng YF, Song XY, Hollings P, Zhou T, Yuan F, Chen LM, Zhang D (2015) Role of asthenosphere and lithosphere in the genesis of the Early Permian Huangshan mafic-ultramafic intrusion in the Northern Tianshan, NW China. Lithos 227:241–254

Deng XH, Wang JB, Pirajno F, Wang YW, Li YC, Li C, Zhou LM, Chen YJ (2016) Re–Os dating of chalcopyrite from selected mineral deposits in the Kalatag district in the eastern Tianshan Orogen, China. Ore Geol Rev 77:72–81

Deng YF, Song XY, Hollings P, Chen LM, Zhou T, Yuan F, Xie W, Zhang D, Zhao BB (2017) Lithological and geochemical constraints on the magma conduit systems of the Huangshan Ni-Cu sulfide deposit, NW China. Mineral Deposita 52:845–862

Eckstrand O, Grinenko L, Krouse H, Paktunc A, Schwann P, Scoates R (1989) Preliminary data on sulphur isotopes and Se/S ratios, and the source of sulphur in magmatic sulphides from the Fox River Sill, Molson Dykes and Thompson nickel deposits, northern Manitoba 1. Current Research Part: C, Geological Survey of Canada, Paper 89-1C: 235–242

Eggins SM, Grün R, McCulloch MT, Pike AWG, Chappell J, Kinsley L, Mortimer G, Shelley M, Murray-Wallace CV, Spötl C, Taylor L

(2005) In situ U-series dating by laser-ablation multi-collector ICP-MS: new prospects for Quaternary geochronology. Quat Sci Rev 24: 2523–2538

Feng YQ, Qian ZZ, Duan J, Sun T, Xu G, Jiang C, Ren M, Chen HJ (2017) Genesis and re-forming potential of mafic-ultramafic intrusions in the western part of east Tianshan Cu-Ni metallogenic belt, Xinjiang. Acta Geol Sin 91:792–811 **(in Chinese with English abstract)**

Feng YQ, Qian ZZ, Duan J, Xu G, Ren M, Jiang C (2018) Geochronological and geochemical study of the Baixintan magmatic Ni-Cu sulphide deposit: new implications for the exploration potential in the western part of the East Tianshan nickel belt (NW China). Ore Geol Rev 95:366–381

Fleet ME, Chryssoulis SL, Stone WE, Weisener CG (1993) Partitioning of platinum-group elements and Au in the Fe–Ni–Cu–S system: experiments on the fractional crystallization of sulfide melt. Contrib Mineral Petrol 115:36–44

Gao JF, Zhou MF (2012) Generation and evolution of siliceous high magnesium basaltic magmas in the formation of the Permian Huangshandong intrusion (Xinjiang, NW China). Lithos 162-163: 128–139

Gao JF, Zhou MF, Lightfoot PC, Wang CY, Qi L, Sun M (2013) Sulfide saturation and magma emplacement in the formation of the Permian Huangshandong Ni-Cu Sulfide Deposit, Xinjiang, Northwestern China. Econ Geol 108:1833–1848

Govindaraju K (1994) Compilation of working values and sample description for 383 geostandards. Geostand Newslett 18:1–158

Han CM, Xiao WJ, Zhao GC, Ao SJ, Zhang JE, Qu WJ, Du AD (2010) In-situ U-Pb, Hf and Re-Os isotopic analyses of the Xiangshan Ni-Cu-Co deposit in Eastern Tianshan (Xinjiang), Central Asia Orogenic Belt: constraints on the timing and genesis of the mineralization. Lithos 120:547–562

Hawkesworth C, Turner S, Peate D, McDermott F, Calsteren P (1997) Elemental U and Th variations in island arc rocks: implications for U-series isotopes. Chem Geol 139:207–221

Hiess J, Bennett VC, Nutman AP, Williams IS (2009) In situ U-Pb, O and Hf isotopic compositions of zircon and olivine from Eoarchaean rocks, West Greenland: new insights to making old crust. Geochim Cosmochim Acta 73:4489–4516

Hofmann AW (1988) Chemical differentiation of the Earth: the relationship between mantle, continental crust, and oceanic crust. Earth Planet Sci Lett 90:297–314

Hu AQ, Jahn B, Zhang GX, Chen YB, Zhang QF (2000) Crustal evolution and Phanerozoic crustal growth in northern Xinjiang: Nd isotopic evidence. Part I. Isotopic characterization of basement rocks. Tectonophysics 328:15–51

Jahn BM, Wu FY, Chen B (2000) Massive granitoid generation in Central Asia: Nd isotope evidence and implication for continental growth in the Phanerozoic. Episodes 23:82–92

Johnson MC, Plank T (1999) Dehydration and melting experiments constrain the fate of subducted sediments. Geochem Geophys Geosyst 1. https://doi.org/10.1029/1999GC000014

Keays RR (1995) The role of komatiitic and picritic magmatism and S-saturation in the formation of ore deposits. Lithos 34:1–18

Keays RR, Lightfoot PC (2010) Crustal sulfur is required to form magmatic Ni-Cu sulfide deposits: evidence from chalcophile element signatures of Siberian and Deccan Trap basalts. Mineral Deposita 45:241–257

Kelemen PB, Hanghøj K, Greene AR (2004) One view of the geochemistry of subduction-related magmatic arcs, with an emphasis on primitive andesite and lower crust. In: Rudnick RL (ed) Treatise on geochemistry, the crust. Elsevier, Amsterdam, pp 593–659

Li CS, Naldrett AJ (1999) Geology and petrology of the Voisey's Bay intrusion: reaction of olivine with sulfide and silicate liquids. Lithos 47:1–31

Li CS, Naldrett AJ (2000) Melting reactions of gneissic inclusions with enclosing magma at Voisey's Bay, Labrador, Canada: implications with respect to ore genesis. Econ Geol 95:801–814

Li CS, Ripley EM (2003) Compositional variations of olivine and sulfur isotopes in the Noril'sk and Talnakh intrusions, Siberia: implications for ore-forming processes in dynamic magma conduits. Econ Geol 98:69–86

Li CS, Ripley EM (2005) Empirical equations to predict the sulfur content of mafic magmas at sulfide saturation and applications to magmatic sulfide deposits. Mineral Deposita 40:218–230

Li CS, Ripley EM (2011) The giant Jinchuan Ni-Cu (PGE) deposit: tectonic setting, magma evolution, ore genesis and exploration implications. Rev Econ Geol 17:163–180

Li C, Naldrett AJ, Ripley EM (2001) Critical factors for the formation of a nickel-copper deposit in an evolved magma system: lessons from a composition of the Pants Lake and Voisey's Bay sulfide occurences in Labrador, Canada. Mineral Deposita 36:85–92

Li CS, Lightfoot PC, Amelin Y, Naldrett AJ (2000) Contrasting petrological and geochemical relationships in the Voisey's Bay and Mushuau intrusions, Labrador, Canada: implications for ore genesis. Econ Geol 95:771–799

Li CS, Xu Z, deWaal SA, Ripley EM, Maier WD (2004) Compositional variations of olivine from the Jinchuan Ni-Cu sulfide deposit, western China: implications for ore genesis. Mineral Deposita 39:159–172

Li JY, Wang KZ, Sun GH, Mo SG, Li WQ, Yang TN, Gao LM (2006a) Paleozoic active margin slices in the southern Turfan Hami basin: geological records of subduction of the Paleo Asian Ocean plate in central Asian regions. Acta Petrol Sin 22:1087–1102 **(in Chinese with English abstract)**

Li JY, Song B, Wang KZ, Li YP, Sun GH, Qi DY (2006b) Permian mafic-ultramafic complexes on the southern margin of the Tu-Ha basin, east Tianshan mountains: geological records of vertical crustal growth in Central Asia. Acta Geosci Sin 27:424–446 **(in Chinese with English abstract)**

Li CS, Naldrett AJ, Ripley EM (2007) Controls on the Fo and Ni contents of olivine in sulfide-bearing mafic/ultramafic intrusions: principles, modeling, and examples from Voisey's Bay. Earth Sci Front 14:177–185

Li X, Wang DK, Zhao SM (2014) The discovery of Baixintan magmatic Ni-Cu sulfide deposits in Hami area, Xinjiang. Xinjiang Geol 32: 466–469 **(in Chinese with English abstract)**

Li CS, Zhang ZW, Li WY, Wang YL, Sun T, Ripley EM (2015) Geochronology, petrology and Hf–S isotope geochemistry of the newly-discovered Xiarihamu magmatic Ni–Cu sulfide deposit in the Qinghai–Tibet plateau, western China. Lithos 216-217:224–240

Lightfoot PC, Hawkesworth CJ (1988) Origin of Deccan Trap lavas: evidence from combined trace element and Sr-, Nd- and Pb-isotope studies. Earth Planet Sci Lett 91:89–104

Lightfoot PC, Hawkesworth CJ (1997) Flood basalts and magmatic Ni, Cu and PGE sulphide mineralization: comparative geochemistry of the Noril'sk (Siberian Trap) and West Greenland sequences: American Geophysical Union Monograph 100: 357–380

Liu DQ, Tang YL, Zhou RH (2005) Copper deposits and nickel deposits in Xinjiang. China. Beijing: Geological Publishing House, 360 p. (in Chinese with English abstract)

Long LL, Wang JB, Wang YW, Fang TH, Mao QG, Gao YH, Zhao LT, Gao LM (2017) Zircon U-Pb geochronological, geochemistry characteristics and potential mineralization significance of the rhyolite in Kalatage copper polymetallic ore cluster area, eastern Tianshan. Acta Prtrologica Sinica 33:367–384 (in Chinese with English abstract)

Ludwig KR (2001) Isoplot/EX, version 2.49. A geochronological toolkit for Microsoft Excel. Berkeley Geochronological Center Special Publication, Berkeley, California, pp 1–55

Ludwig KR (2012) Isoplot 3.75–4.15: a geochronological toolkit for Microsoft Excel. Berkeley Geochronology Center Special Publication, Berkeley, California, pp 1–75

Ma RS, Wang CY, Ye SF, Liu GB (1993) Tectonic framework and crustal evolution of the Eastern Tianshan. Nanjing University Press, Nanjing (in Chinese)

Maier WD, Barnes SJ (2010) The Kabanga Ni sulfide deposits, Tanzania: II. Chalcophile and siderophile element geochemistry. Mineral Deposita 45:443–460

Maier WD, Li C, De Waal SA (2001) Why are there no major Ni-Cu sulfide deposits in large layered mafic-ultramafic intrusions. Can Mineral 39:547–556

Maier WD, Barnes SJ, Chinyepi G, Barton JJ, Eglington B, Setshedi T (2008) The composition of magmatic Ni-Cu-(PGE) sulfide deposits in the Tati and Selebi-Phikwe belts of eastern Botswana. Mineral Deposita 43:37–60

Mao JW, Yang JM, Qu WJ, Du AD, Wang ZL, Han CM (2002) Re-Os dating of Cu-Ni sulfide ores from Huangshandong deposit in Xinjiang and its geodynamic significance. Mineral Deposits 21: 323–330 (in Chinese with English abstract)

Mao JW, Pirajno F, Zhang ZH, Chai FM, Wu H, Chen SP, Chen LS, Yang JM, Zhang CQ (2008) A review of the Cu-Ni sulphide deposits in the Chinese Tianshan and Altay orogens (Xinjiang Autonomous Region, NW China): principal characteristics and ore-forming processes. J Asian Earth Sci 32:184–203

Mao QG, Fang TH, Wang JB, Wang SL, Wang N (2010) Geochronology studies of the Early Paleozoic Honghai massive sulfide deposits and its geological significance in Kalatage area, eastern Tianshan Mountain. Acta Petrol Sin 26:2017–2026 (in Chinese with English abstract)

Mao YJ, Qin KZ, Li CS, Xue SC, Ripley EM (2014) Petrogenesis and ore genesis of the Permian Huangshanxi sulfide ore-bearing mafic-ultramafic intrusion in the Central Asian Orogenic Belt, western China. Lithos 200-201:111–125

Mao YJ, Qin KZ, Li CS, Tang DM (2015) A modified genetic model for the Huangshandong magmatic sulfide deposit in the Central Asian Orogenic Belt, Xinjiang, western China. Mineral Deposita 50:65–82

Mao YJ, Qin KZ, Barnes SJ, Tang DM, Xue SC, Vaillant ML (2017a) Genesis of the Huangshannan high-Ni tenor magmatic sulfide deposit in the Eastern Tianshan, northwest China: constraints from PGE geochemistry and Os–S isotopes. Ore Geol Rev 90:591–606

Mao QG, Yu MJ, Xiao WJ, Windley BF, Li YC, Wei XF, Zhu JJ, Lv XQ (2017b) Skarn-mineralized porphyry adakites in the Harlik arc at Kalatage, E. Tianshan (NW China): slab melting in the Devonian-early Carboniferous in the southern Central Asian Orogenic Belt. J Asian Earth Sci. https://doi.org/10.1016/j.jseaes.2017.03.021

Mattinson JM (2005) Zircon U-Pb chemical abrasion ("CA-TIMS") method: combined annealing and multi-step partial dissolution analysis for improved precision and accuracy of zircon ages. Chem Geol 220:47–66

Mavrogenes JA, O'Neill HSC (1999) The relative effects of pressure, temperature and oxygen fugacity on the solubility of sulfide in mafic magmas. Geochim Cosmochim Acta 63:1173–1180

Naldrett AJ (1994) Proceedings of the Sudbury ± Noril'sk Symposium. Ontario Geological Survey Epec 5:423

Naldrett AJ (1997) Key factors in the genesis of Noril'sk, Sudbury, Jinchuan, Voisey's Bay and other world-class Ni-Cu-PGE deposits: implications for exploration. Aust J Earth Sci 44:283–315

Naldrett AJ (1999) World-class Cu-Ni-PGE deposits: key factors in their genesis. Mineral Deposita 34:227–240

Naldrett AJ, Innes DC, Sowa J, Gorton MP (1982) Compositional variations within and between five Sudbury ore deposits. Econ Geol 77: 1519–1534

Ohmoto H, Rye RO (1979) Isotopes of sulfur and carbon. In: Barnes HL (ed) Geochemistry of hydrothermal ore deposits, 2nd edn. John Wiley and Sons, London, pp 509–567

Peach CL, Mathez EA, Keays RR (1990) Sulfide melt-silicate melt distribution coefficients for noble metals and other chalcophile elements as deduced from MORB: implications for partial melting. Geochim Cosmochim Acta 54:3379–3389

Pearce JA (1982) Trace elements characteristics of lavas from destructive plate boundaries. In: Thorpe RS (ed) Andesites: orogenic andesites and related rocks. Wiley, New York, pp 525–548

Pearce JA (1983) The role of sub-continental lithosphere in magma genesis at destructive plate margins. In: Hawkesworth CJ, Norry MJ (eds) Continental basalts and mantle xenoliths. Shiva, Nantwich, pp 230–249

Pettigrew N, Hattori K (2006) The Quetico Intrusions of Western Superior Province: Neo-Archean examples of Alaskan/Ural-type mafic-ultramafic intrusions. Precambrian Res 149:21–42

Qi L, Hu J, Gregoire DC (2000) Determination of trace elements in granites by inductively coupled plasma mass spectrometry. Talanta 51:507–513

Qi L, Zhou MF, Wang CY (2004) Determination of low concentrations of platinum group elements in geological samples by ID-ICP-MS. J Anal At Spectrom 19:1335–1339

Qi L, Zhou MF, Wang CY, Sun M (2007) Evaluation of the determination of Re and PGEs abundances of geological samples by ICP-MS coupled with a modified Carius tube digestion at different temperatures. Geochem J 41:407–414

Qin KZ, Fang TH, Wang SL, Zhu BQ, Feng YM, Yu HF, Xiu QY (2002) Plate tectonics division, evolution and metallogenic settings in eastern Tianshan mountains, NW-China. Xinjiang Geol 20:302–308 (in Chinese with English abstract)

Qin KZ, Zhang LC, Xiao WJ, Xu XW, Yan Z, Mao JW (2003) Overview of major Au, Cu, Ni and Fe deposits and metallogenic evolution of the eastern Tianshan Mountains, Northwestern China. In: Mao JW, Goldfarb R, Seltmann R, Wang DH, Xiao WJ, Hart C (eds) Tectonic evolution and metallogeny of the Chinese Altay and Tianshan, vol 10. IAGOD Guidebook Series, London, pp 227–248

Qin KZ, Sun BX, Sakyi PA, Tang DM, Li XH, Sun H, Xiao QH, Liu PP (2011) SIMS zircon U-Pb geochronology and Sr-Nd isotopes of Ni-Cu-bearing mafic-ultramafic intrusions in Eastern Tianshan and Beishan in correlation with flood basalts in Tarim basin (NW China): constraints on a ca. 280 Ma mantle plume. Am J Sci 311: 237–260

Ren MH, Wang CY, Ni K, Sun YL (2013) Differentiation of magmas in the formation of Permian mafic-ultramafic intrusions in the Dacaotan area, Eastern Tianshan: implications for Ni-Cu-(PGE) sulfide mineralization potentials. Acta Petrol Sin 29:3473–3486 (in Chinese with English abstract)

Ripley EM (2009) Magmatic sulfide mineralization in Alaskan-type complexes. In: Li CS, Ripley EM (eds) New development in magmatic Ni-Cu and PGE deposits, vol 7. Geological Publishing House, Beijing, pp 219–228

Ripley EM, Li CS (2013) Sulfide saturation in mafic magmas: is external sulfur required for magmatic Ni-Cu-(PGE) ore genesis? Econ Geol 108:45–58

Ripley EM, Li C, Shin D (2002) Paragneiss assimilation in the genesis of magmatic Ni-Cu-Co sulfide mineralization at Voisey's Bay, Labrador: $\delta^{34}S$, $\delta^{13}C$, and Se/S evidence. Econ Geol 97:1307–1318

Robertson JC, Ripley EM, Barnes SJ (2015) Sulfur liberation from country rocks and incorporation in mafic magmas. Econ Geol 110:1111–1123

Roeder PL, Emslie RF (1970) Olivine-liquid equilibrium. Contrib Mineral Petrol 29:275–289

Rudnick R, Gao S (2003) The role of lower crustal recycling in continent formation. Geochim Cosmochim Acta 67:403

San JZ, Qin KZ, Tang DM, Su BX, Sun H, Xiao QH, Liu PP, Cao MJ (2010) Precise zircon U-Pb ages of Tulargen large Cu-Ni-ore bearing mafic-ultramafic complex and their geological implications. Acta Petrol Sin 26:3027–3035 (in Chinese with English abstract)

Seat Z, Beresford SW, Grguric BA, Mary Gee MA, Gressineau NV (2009) Reevaluation of the role of external sulfur addition in the genesis of Ni-Cu-PGE deposits: evidence from the Nebo-Babel Ni-Cu-PGE deposit, West Musgrave, Western Australia. Econ Geol 104:521–538

Sengör AMC, Natal'in BA, Burtman VS (1993) Evolution of the Altaid tectonic collage and Paleozoic crustal growth in Asia. Nature 364: 299–307

Shu LS, Wang B, Zhu WB, Guo ZJ, Charvet J, Zhang Y (2010) Timing of initiation of extension in the Tianshan, based on structural, geochemical and geochronological analyses of bimodal volcanism and olistostrome in the Bogda Shan (NW China). International Journal of Earth Sciences (Geol Rundsch) 100:1647–1663. https://doi.org/10.1007/s00531-010-0575-5

Song XY, Li XR (2009) Geochemistry of the Kalatongke Ni–Cu–(PGE) sulfide deposit, NW China: implications for the formation of magmatic sulfide mineralization in a postcollisional environment. Mineral Deposita 44:303–327

Song XY, Xie W, Deng YF, Crawford AJ, Zheng WQ, Zhou GF, Deng G, Chen SL, Li J (2011) Slab break-off and the formation of Permian mafic-ultramafic intrusions in southern margin of Central Asian Orogenic Belt, Xinjiang, NW China. Lithos 127:128–143

Song XY, Chen LM, Deng YF, Xie W (2013) Syncollisional tholeiitic magmatism induced by asthenosphere upwelling owing to slab detachment at the southern margin of the Central Asian Orogenic Belt. J Geol Soc Lond 170:941–950

Song XY, Yi JN, Chen LM, She YW, Liu CZ, Dang XY, Yang QA, Wu SK (2016) The giant Xiarihamu Ni-Co sulfide deposit in the East Kunlun orogenic belt, northern Tibet plateau, China. Econ Geol 111: 29–55

Su CQ, Jiang CY, Xia MZ, Zhang L, Ji HG, Guo FF, Liu XJ (2008) Zircon SHRIMP U-Pb dating from granites of the metamorphic core complex system in Jueluotage tectonic belt and its geological significance. Acta Petrol Sin 24:2789–2799 (in Chinese with English abstract)

Su BX, Qin KZ, Sakyi PA, Li XH, Yang YH, Sun H, Tang DM, Liu PP, Xiao QH, Malaviarachchi SP (2011) U-Pb ages and Hf-O isotopes of zircons from Late Paleozoic mafic-ultramafic units in the southern Central Asian Orogenic Belt: tectonic implications and evidence for an Early-Permian mantle plume. Gondwana Res 20:516–531

Su BX, Qin KZ, Su H, Tang DM, Sakyi PA, Chu ZY, Liu PP, Xiao QH (2012) Subduction-induced mantle heterogeneity beneath Eastern Tianshan and Beishan: insights from Nd-Sr-Hf-O isotopic mapping of Late Paleozoic mafic-ultramafic complexes. Lithos 134-135:41–51

Su BX, Qin KZ, Tang DM, Sakyi PA, Liu PP, Su H, Xiao QH (2013) Late Paleozoic mafic-ultramafic intrusions in southern Central Asian Orogenic Belt (NW China): insight into magmatic Ni-Cu sulfide mineralization in orogenic setting. Ore Geol Rev 51:57–73

Sun SS, McDonough W (1989) Chemical and isotopic systematics of oceanic basalts: implications for mantle composition and processes. Geol Soc Lond, Spec Publ 42:313–345

Sun T, Qian ZZ, Deng YF, Li CS, Song XY, Tang QY (2013) PGE and isotope (Hf-Sr-Nd-Pb) constraints on the origin of the Huangshandong magmatic Ni-Cu sulfide deposit in the Central Asian Orogenic Belt, Northwestern China. Econ Geol 108:1849–1864

Tang DM, Qin KZ, Sun H, Su BX, Xiao QH (2012) The role of crustal contamination in the formation of Ni-Cu sulfide deposits in Eastern Tianshan, Xinjiang, Northwest China: evidence from trace element geochemistry, Re-Os, Sr-Nd, zircon Hf-O, and sulfur isotopes. J Asian Earth Sci 49:145–160

Tang DM, Qin KZ, Su BX, Sakyi PA, Mao YJ, Xue SC (2014) Petrogenesis and mineralization of the Hulu Ni-Cu sulphide deposit in Xinjiang, NW China: constraints from Sr-Nd isotopic and PGE compositions. Int Geol Rev 56:711–733

Thakurta J, Ripley EM, Li CS (2008) Geochemical constraints on the origin of sulfide mineralization in the Duke Island Complex, southeastern Alaska. Geochem Geophys Geosyst 9:Q07003

Tornos F, Casquet C, Galindo C, Velasco F, Canales A (2001) A new style of Ni-Cu mineralization related to magmatic breccia pipes in a transpressional magmatic arc, Aguablanca, Spain. Mineral Deposita 36(7):700–706

Wang YL, Zhang ZW, You MX, Li X, Li K, Wang BL (2015) Chronological and geochemical characteristics of the Baixintan Ni-Cu deposit in Eastern Tianshan Mountains, Xinjiang, and their implications for Ni-Cu mineralization. Geol China 42:452–467 (in Chinese with English abstract)

Wang YH, Zhang FF, Liu JJ, Que CY (2016a) Carboniferous magmatism and mineralization in the area of the Fuxing Cu deposit, Eastern Tianshan, China: evidence from zircon U–Pb ages, petrogeochemistry, and Sr–Nd–Hf–O isotopic compositions. Gondwana Res 34:109–128

Wang YL, Zhang ZW, Zhang JW, You MX, Li K, Wang BL (2016b) Mineralogy and Sr-Nd isotope characteristics of Baixintan Ni-Cu deposit in eastern Tianshan mountains, Xinjiang, and mineralization process. Acta Geol Sin 90:2747–2758 (in Chinese with English abstract)

Wendlandt R (1982) Sulfide saturation of basalt and andesite melts at high pressures and temperatures. Am Mineral 67:877–885

Wiedenbeck M, Alle P, Corfu F, Griffin WL, Meier M, Oberli F, Quadt AV, Roddick JC, Spiegel W (1995) Three natural zircon standards for U-Th-Pb, Lu-Hf, trace element and REE analyses. Geostand Geoanal Res 19:1–23

Wilson M (1989) Igneous petrogenesis. Unwin Hyman, London, pp 1–466

Windley BF, Alexeiev D, Xiao WJ, Kröner A, Badarch G (2007) Tectonic models for accretion of the Central Asian Orogenic Belt. J Geol Soc Lond 164:31–47

Windrim DP, Mcculloch MT (1986) Nd and Sr isotopic systematics of central Australian granulites: chronology of crustal development and constraints on the evolution of lower continental crust. Contrib Mineral Petrol 94:289–303

Xiao WJ, Zhang LC, Qin KZ, Sun S, Li JL (2004) Paleozoic accretionary and collisional tectonics of the eastern Tianshan (China): implications for the continental growth of central Asia. Am J Sci 304: 370–395

Xiao WJ, Han CM, Yuan C, Sun M, Lin SF, Chen HL, Li ZL, Li JL, Sun S (2008) Middle Cambrian to Permian subduction-related accretionary orogenesis of Northern Xinjiang, NW China: implications for the tectonic evolution of central Asia. J Asian Earth Sci 32:102–117

Xie W, Song XY, Chen LM, Deng YF, Zheng WQ, Wang YS, Ba DH, Zhang XQ, Luan Y (2014) Geochemistry insights on the genesis of the subduction-related Heishan magmatic Ni-Cu-(PGE) deposit in Gansu, NW China, at the southern margin of the Central Asian Orogenic Belt. Econ Geol 109:1563–1583

Xie W, Xu YG, Chen YB, Luo ZY, Hong LB, Ma L, Liu HQ (2016a) High-alumina basalts from the Bogda Mountains suggest an arc setting for Chinese Northern Tianshan during the Late Carboniferous. Lithos 256-257:165–181

Xie W, Luo ZY, Xu YG, Chen YB, Hong LB, Ma L, Ma Q (2016b) Petrogenesis and geochemistry of the Late Carboniferous rear-arc (or back-arc) pillow basaltic lava in the Bogda Mountains, Chinese North Tianshan. Lithos 244:30–42

Yang YH, Zhang FH, Chu ZY, Xie XW, Wu FY (2010) Combined chemical separation of Lu, Hf, Rb, Sr, Sm and Nd from a single rock digest and precise and accurate isotope determinations of Lu-Hf, Rb-Sr and Sm-Nd isotope systems using multi-collector ICP-MS and TIMS. Int J Mass Spectrom 290:120–126

Yang WZ, Ren Y, Tian JT, She JZ, Yang GG (2017) The discovery of Lubei Cu-Ni sulfide deposit in eastern Tianshan, NW China and its

significant. Bulletin of Mineraloy, Petrology and Geochemistry 36: 112–120 (in Chinese with English abstract)

Yuan F, Zhou TF, Fan Y, Tan LG, David C, Sebastien M, Wang QM, Wang WJ (2007) LA-ICPMS U-Pb age of zircon from basalt of Matoutan Group in Shilipo native copper mineralized area, Eastern Tianshan, Xinjiang. Acta Petrol Sin 23:1973–1980 (in Chinese with English abstract)

Zhang LC, Xiao WJ, Qin KZ, Zhang Q (2006) The adakite connection of the Tuwu-Yandong copper porphyry belt, eastern Tianshan, NW China: trace element and Sr-Nd-Pb isotope geochemistry. Mineral Deposita 41:188–200

Zhang M, Stephenson PJ, O'Reilly SY, McCulloch M, Norman M (2001) Petrogenesis and geodynamic implications of Late Cenozoic basalts in north Queensland, Australia: trace-element and Sr–Nd–Pb isotope evidence. J Petrol 42:685–719

Zhang MJ, Li CS, Fu PE, Hu PQ, Ripley EM (2011) The Permian Huangshanxi Cu-Ni deposit in western China: intrusive-extrusive association, ore genesis, and exploration implications. Mineral Deposita 46:153–170

Zhang DY, Zhou TF, Yuan F, Fiorentini ML, Said N, Lu YJ, Pirajno F (2013) Geochemical and isotopic constraints on the genesis of the Jueluotage native copper mineralized basalt, Eastern Tianshan, Northwest China. J Asian Earth Sci 73:317–333

Zhang DY, Zhou TF, Yuan F, Fan Y, Deng YF, Xu C, Zhang RF (2014) Genesis of Permian granites along the Kangguer Shear Zone, Jueluotage area, Northwest China: geological and geochemical evidence. Lithos 198-199:141–152

Zhao Y, Xue CJ, Zhao XB, Yang YQ, Ke JJ (2015) Magmatic Cu-Ni sulfide mineralization of the Huangshannan mafic-untramafic intrusion, Eastern Tianshan, China. J Asian Earth Sci 105:155–172

Zhao Y, Xue CJ, Zhao XB, Yang YQ, Ke JJ, Zu B, Zhang GZ (2016) Origin of an anomalously Ni-rich parental magma and genesis of the Huangshannan Ni-Cu sulfide deposit, Central Asian Orogenic Belt, Northwestern China. Ore Geol Rev 77:57–71

Zhao BB, Deng YF, Zhou TF, Yuan F, Zhang DY, Deng G, Li WD, Li Y (2018) Petrogenesis of the Baixintan Ni-Cu sulfide-bearing mafic-ultramafic intrusion, east Tianshan: evidence from geochronology, petrogeochemistry and Sr-Nd isotope. Acta Petrol Sin 34(9):2733–2753 (in Chinese with English abstract)

Zhou MF, Lesher CM, Yang ZX, Li JW, Sun M (2004) Geochemistry and petrogenesis of 270 Ma Ni-Cu-(PGE) sulfide-bearing mafic intrusions in the Huangshan District, eastern Xinjiang, Northwest China: implications for the tectonic evolution of the Central Asian orogenic belt. Chem Geol 209:233–257

Zhou TF, Yuan F, Zhang DY, Fan Y, Liu S, Peng MX, Zhang JD (2010) Geochronology, tectonic setting and mineralization of granitoids in Jueluotage area, eastern Tianshan, Xinjiang. Acta Petrol Sin 26: 478–502 (in Chinese with English abstract)

Zindler A, Hart S (1986) Chemical geodynamics. Annu Rev Earth Planet Sci 14:493–571